



OPEN ACCESS

EDITED BY

Aline Bozec,
University of Erlangen Nuremberg, Germany

REVIEWED BY

Janos G. Filep,
Montreal University, Canada
Celio Geraldo Freire-de-Lima,
Federal University of Rio de Janeiro, Brazil

*CORRESPONDENCE

Philip A. Efron
✉ philip.efron@surgery.ufl.edu
Rhonda Bacher
✉ rbacher@ufl.edu

[†]These authors have contributed equally to this work and share first authorship

RECEIVED 13 December 2023

ACCEPTED 09 April 2024

PUBLISHED 24 April 2024

CITATION

Barrios EL, Leary JR, Darden DB, Rincon JC, Willis M, Polcz VE, Gillies GS, Munley JA, Dirain ML, Ungaro R, Nacionales DC, Gauthier M-PL, Larson SD, Morel L, Loftus TJ, Mohr AM, Maile R, Kladdé MP, Mathews CE, Brusko MA, Brusko TM, Moldawer LL, Bacher R and Efron PA (2024) The post-septic peripheral myeloid compartment reveals unexpected diversity in myeloid-derived suppressor cells. *Front. Immunol.* 15:1355405. doi: 10.3389/fimmu.2024.1355405

COPYRIGHT

© 2024 Barrios, Leary, Darden, Rincon, Willis, Polcz, Gillies, Munley, Dirain, Ungaro, Nacionales, Gauthier, Larson, Morel, Loftus, Mohr, Maile, Kladdé, Mathews, Brusko, Brusko, Moldawer, Bacher and Efron. This is an open-access article distributed under the terms of the [Creative Commons Attribution License \(CC BY\)](https://creativecommons.org/licenses/by/4.0/). The use, distribution or reproduction in other forums is permitted, provided the original author(s) and the copyright owner(s) are credited and that the original publication in this journal is cited, in accordance with accepted academic practice. No use, distribution or reproduction is permitted which does not comply with these terms.

The post-septic peripheral myeloid compartment reveals unexpected diversity in myeloid-derived suppressor cells

Evan L. Barrios^{1†}, Jack R. Leary^{2†}, Dijoia B. Darden¹, Jaimar C. Rincon¹, Micah Willis¹, Valerie E. Polcz¹, Gwendolyn S. Gillies¹, Jennifer A. Munley¹, Marvin L. Dirain¹, Ricardo Ungaro¹, Dina C. Nacionales¹, Marie-Pierre L. Gauthier³, Shawn D. Larson¹, Laurence Morel⁴, Tyler J. Loftus¹, Alicia M. Mohr¹, Robert Maile¹, Michael P. Kladdé³, Clayton E. Mathews⁵, Maigan A. Brusko⁵, Todd M. Brusko⁵, Lyle L. Moldawer¹, Rhonda Bacher^{2*} and Philip A. Efron^{1*}

¹Sepsis and Critical Illness Research Center, Department of Surgery, University of Florida College of Medicine, Gainesville, FL, United States, ²Department of Biostatistics, University of Florida College of Medicine and Public Health and Health Sciences, Gainesville, FL, United States, ³Department of Biochemistry and Molecular Biology, University of Florida College of Medicine, Gainesville, FL, United States, ⁴Department of Microbiology and Immunology, University of Texas San Antonio School of Medicine, San Antonio, TX, United States, ⁵Department of Pathology, Immunology and Laboratory Medicine, University of Florida College of Medicine, Gainesville, FL, United States

Introduction: Sepsis engenders distinct host immunologic changes that include the expansion of myeloid-derived suppressor cells (MDSCs). These cells play a physiologic role in tempering acute inflammatory responses but can persist in patients who develop chronic critical illness.

Methods: Cellular Indexing of Transcriptomes and Epitopes by Sequencing and transcriptomic analysis are used to describe MDSC subpopulations based on differential gene expression, RNA velocities, and biologic process clustering.

Results: We identify a unique lineage and differentiation pathway for MDSCs after sepsis and describe a novel MDSC subpopulation. Additionally, we report that the heterogeneous response of the myeloid compartment of blood to sepsis is dependent on clinical outcome.

Discussion: The origins and lineage of these MDSC subpopulations were previously assumed to be discrete and unidirectional; however, these cells exhibit a dynamic phenotype with considerable plasticity.

KEYWORDS

myeloid-derived suppressor cells, sepsis, transcriptomics, single-cell RNA sequencing, chronic critical illness

1 Introduction

Sepsis is defined as life-threatening organ dysfunction caused by a dysregulated host response to infection (1), with survivors experiencing either a rapid recovery or chronic critical illness (CCI) (2). The emergency myelopoietic response to sepsis is characterized by hematopoietic stem and progenitor cell (HSPC) expansion and preferential differentiation along myeloid pathways (3–7). We and others have previously demonstrated that sepsis induces an expansion of circulating myeloid-derived suppressor cells (MDSCs), and that both an increase in and persistence of specific MDSC subpopulations are seen in sepsis patients with poor clinical outcomes (4, 8, 9).

Three MDSC subpopulations are typically described based on cell surface expression, mechanisms of immune suppression, and inflammatory profiles: granulocytic (PMN-), monocytic (M-), and early (E-) MDSCs (10, 11). Although these MDSCs differ phenotypically, they are all capable of suppressing T-lymphocyte proliferation (4, 12). As research into the myeloid compartment during inflammation expands, the complexity of intermediate cell types is just beginning to be understood. Indeed, Hegde et al. recently concluded that suppressive myeloid cell types, including MDSCs, “are highly heterogeneous and context dependent” (13). The authors presented an emergent view of MDSCs that emphasizes heterogeneity and plasticity in contrast to the classical view of MDSCs as the midpoint in a differentiation pathway that results in terminally-differentiated monocytes and granulocytes (13).

Single-cell RNA-sequencing (scRNA-seq) details the transcriptomes of complex and heterogeneous cell mixtures. An extension of this technique, Cellular Indexing of Transcriptomes and Epitopes by Sequencing (CITE-seq), simultaneously profiles cell surface proteins for each cell. We initially performed CITE-seq in order to identify MDSC subpopulations based on cell surface markers/cell phenotypes, as our previous results (14) indicated that MDSCs from septic patients may not express some of the classic genes found in MDSCs from cancer patients, making them difficult to identify. We compared the transcriptomes of myeloid cells from healthy subjects, acutely septic patients, and patients with good and poor clinical outcomes at later time points after sepsis. We found that MDSC subpopulations evolve over time and that outcome-dependent MDSC subpopulations exist. Specifically, we identified a novel hybrid (H)-MDSC phenotype unique to some sepsis survivors with poor clinical outcomes as well as acutely septic patients that progressed to CCI. Additionally, our findings suggest that the proliferation and cytokine production of lymphocytes, when co-cultured with MDSCs, vary at different time points after sepsis. Importantly, MDSCs do not express key genes seen in cancer whose downstream products suppress T-cell responsiveness. Overall, our results demonstrate a critical need for disease- or “context-” specific understanding of MDSCs when considering host-specific immune dysfunction and potential therapies.

2 Materials and methods

2.1 Study design

Our study design was previously reported by Darden et al. (14). To summarize, this prospective, observational cohort study was

registered with *clinicaltrials.gov* (NCT02276417) and conducted at a tertiary care, academic research hospital. The objective of the study was to better understand the myeloid response (specifically blood MDSCs) to acute sepsis, and to identify transcriptomic differences in sepsis patients who rapidly recover versus those who develop CCI. Our hypothesis was that differences in the myeloid transcriptomic landscape could explain why some sepsis patients rapidly recover while others develop CCI.

Sepsis designation occurred through an electronic medical record-based Modified Early Warning Signs-Sepsis Recognition System (MEWS-SRS), which uses white blood cell count, heart rate, respiration rate, blood pressure, and mental status to identify patients at risk for sepsis. All patients with sepsis were treated with early goal-directed fluid administration, initiation of broad-spectrum antibiotics, and vasopressor administration if appropriate. Antibiotic treatment was tailored to culture results and antibiotic resistance information.

Inclusion criteria:

- Admission to the intensive care unit (ICU).
- Age >17 years.
- Diagnosis of sepsis or septic shock according to the 2016 SCIM/ESICM International Sepsis Definitions Conference (1).
- Initial septic episode while hospitalized.
- Management of patient via the sepsis clinical management protocol (15).

Exclusion criteria:

- Refractory shock.
- Inability to achieve source control.
- Pre-sepsis expected lifespan <3 months.
- Expected withdrawal of care.
- Severe congestive heart failure (NYHA Class IV).
- Child-Pugh Class C liver disease or undergoing evaluation for liver transplant.
- HIV infection with CD4⁺ count <200 cells/mm³.
- Prior organ transplant, use of chronic steroids, or immunosuppressive agents.
- Pregnancy.
- Institutionalized or other vulnerable patients.
- Chemotherapy or radiotherapy treatment within 30 days of sepsis onset.
- Severe traumatic brain injury (defined by radiologic evidence and GCS <8).
- Spinal cord injury with permanent deficits.
- Unable to obtain informed consent.

CCI was defined as ICU length of stay >13 days with persistent organ dysfunction as measured by the Sequential Organ Failure Assessment (SOFA) score. Patients were also designated CCI with <14 days ICU length of stay if they were transferred to another hospital, or discharged to a long-term acute care facility or hospice with evidence of persistent organ dysfunction (4, 16).

2.2 Human blood collection and sample preparation

Whole blood samples were collected at the following time points: 4 ± 1 days and 14-21 days after sepsis (16). For the former, we enrolled 4 patients diagnosed with septic shock (1) in order to guarantee a strong host response and transcriptomic alterations in circulating leukocytes. Interestingly, only half of these septic shock patients went on to develop CCI (17, 18). Samples from 5 patients who developed CCI and 4 patients who rapidly recovered after sepsis were obtained from additional patients between 14-21 days after sepsis diagnosis. We previously determined this time point to be key to MDSC differentiation as well as distinguishing CCI from rapid recovery (4, 16). In addition, whole blood was collected from 12 healthy subjects (1, 2). The proportion of men and women did not differ between sepsis patients and healthy subjects (Table 1). Healthy subjects trended towards being younger than sepsis patients, although they still met the criteria of middle age (>45 years), encompassing patients who have poor outcomes after sepsis compared to younger cohorts (17, 18). Healthy subjects and septic patients had similar underlying comorbidities (most commonly hypertension, chronic obstructive pulmonary disease, and diabetes mellitus).

Each blood collection underwent two enrichment procedures. Peripheral blood mononuclear cells (PBMCs) were collected from half of each sample using Ficoll-Paque™ PLUS (Millipore Sigma, St. Louis, MO) and density gradient centrifugation. Myeloid cells were collected using the RosetteSep™ HLA Myeloid Cell Enrichment Kit (STEMCELL Technologies, Vancouver). A 1:3 mixture of enriched PBMCs: myeloid cells was created in order to adequately analyze the small target population (MDSCs, especially in healthy subjects) while also allowing for characterization of other important immune cell populations using CITE-seq.

2.2.1 Human T-cell isolation and proliferation assay

Total T cells in the PBMC suspension were captured by immunomagnetic negative selection using EasySep™ Human T Cell

Isolation Kits (STEMCELL Technologies, Vancouver) according to the manufacturer's instructions. Isolated CD3⁺ lymphocytes were labeled with cell trace violet (Thermo Fisher, Waltham, MA) to assess T-cell proliferation. T lymphocytes (1×10^5 CD3⁺) were seeded into a 96-well plate and stimulated with soluble anti-CD3/CD28 antibodies (STEMCELL Technologies, Vancouver) or without, which served as the control. CD66b⁺ cells were also isolated from the PBMC fractions using EasySep™ positive selection kits (STEMCELL Technologies, Vancouver) and were co-cultured with stimulated T cells in a 1:1 ratio at 37°C and 5% CO₂. After 4 days, cells were harvested and supernatants were obtained for cytokine analysis. Cells were stained with anti-CD8 FITC and anti-CD4 PE and analyzed via flow cytometry (ZE5 Cell Analyzer, Bio-Rad Laboratories, CA). Proliferation indices were calculated as the total number of cell divisions divided by the number of cells that went into division (considering cells that underwent at least one division).

2.2.2 Cytokine analysis

Human high sensitivity T cell magnetic bead 6-plex panels (IFN- γ , IL-10, IL-12 (p70), IL-17 α , IL-2, IL-23) were purchased from EMD Millipore (Billerica, MA). Supernatants after cell culture were used for T cell-associated cytokines. xPONENT software (EMD Millipore, Billerica, MA) was used for cytokine analysis.

2.2.3 Flow cytometry

PBMC samples were analyzed fresh (not frozen and rethawed) due to differential viability of cell populations, particularly granulocytes (19, 20). Although the PBMC fraction excludes mature granulocytes, it does contain low-density granulocytes that are presumed to include PMN-MDSCs (21). Classically, human blood MDSCs are defined from PBMCs as: M-MDSCs (CD11b⁺CD14⁺CD33⁺HLA-DR^{low/-}) and PMN-MDSCs (CD11b⁺CD15⁺HLA-DR^{low}CD66b⁺) (22). Our preliminary flow cytometric analysis revealed that CD15 was not a good cell surface marker to isolate CD14⁺ cells from PBMCs (Figure S1C). In fact, the analysis of CD33⁺CD11b⁺HLA-DR^{low/-} cells revealed heterogeneity in CD14 and CD15 cell surface expression. Thus, we chose

TABLE 1 Patient characteristics between cohorts.

	Healthy Subjects (n=12)	Sepsis Day 4 \pm 1 (n=4)	RAP Days 14-21 (n=4)	CCI Days 14-21 (n=5)	p-value
Male, # (%)	7 (58)	1 (25)	1 (25)	3 (60)	0.48
Age in years, ($\mu \pm$ SD)	46 \pm 10	67 \pm 22	61 \pm 16	58 \pm 18	0.08
BMI ($\mu \pm$ SD)		39 \pm 19	37 \pm 20	21 \pm 3	0.19
Septic shock, # (%)		4 (100)	1 (25)	4 (80)	
CCI (median)		5.5	2	2	
Comorbidities (#)	Cancer (1), COPD (1), DM (1), HTN (3)	COPD (1), DM (2), HTN (4)	COPD (1), DM (1), HTN (4)	DM (1), HTN (2)	
Admission Diagnosis (#)		NSTI (1), Cholelithiasis (1), SBO (1), Planned operation (1)	NSTI (2), SBO (2)	Planned operation (1), Complication (1), Intra-abdominal abscess (1), Pancreatitis (1), MCC (1)	

Cohorts are healthy subjects, acutely septic patients, and late sepsis patients who experienced rapid recovery (RAP) and chronic critical illness (CCI). BMI, body mass index; CCI, Charlson comorbidity index; COPD, chronic obstructive pulmonary disease; DM, diabetes mellitus; HTN, hypertension; NSTI, necrotizing soft tissue infection; SBO, small bowel obstruction; MCC, Motorcycle crash.

to isolate CD66b⁺ cells from PBMCs to obtain PMN-MDSCs (Figure S1C).

2.3 Statistics

2.3.1 scRNA-seq read preprocessing

Gene expression and feature-barcoding data were generated using 10x Genomics v1.1 5' chemistry and were sequenced on an Illumina HiSeq[®] with a target of 10,000 cells per sample (23). The Cell Ranger (10X Genomics) software suite was used to process base calls into FASTQ files, which were checked for quality control aberrations using FastQC v0.11.7 (24). A spliced + intronic, or *splice*, reference transcriptome was generated from the hg38 reference genome (25). Reads were pseudoaligned to the reference transcriptome with alevin-fry v0.8.1; USA mode was used for gene expression reads in order to provide separate quantifications of spliced, unspliced, and ambiguous mRNA abundance (26–28). The counts of 11 cell surface proteins of interest were also quantified using alevin-fry. Splicing-aware gene expression quantification was performed using Ensembl transcript IDs, with final counts matrices aggregated using Ensembl gene IDs.

2.3.2 scRNA-seq data processing

Downstream data processing and analysis were performed primarily in R v4.2.3, with some additional processes written in Python v3.8 as required (29, 30). After loading the unfiltered spliced, unspliced, and ambiguous mRNA counts into R using fishpond package v2.4.1, we defined total mRNA counts as the elementwise sum of all three counts matrices and added the ambiguous counts to the spliced counts matrix (31). Unless otherwise specified, total mRNA counts were used as input throughout the analysis. Empty droplets and ambient mRNA were then identified and filtered out using the DropletUtils package v1.18.1 (32, 33). Cells with an estimated false discovery rate of <0.01 were kept for each sample. Next, the percentage of spliced reads coming from mitochondrial genes was computed for each cell, and cells with less than 5% mitochondrial DNA were kept (no significant difference between healthy and septic samples). Cell surface protein counts were imported as well, and cells that had valid gene expression barcodes but not protein barcodes were assigned a value of “0” for each protein. The raw counts matrices were then formatted and merged using the Seurat package v4.3.0, providing a single object with total, unspliced, and spliced mRNA as well as cell surface protein assays (34). Cells with less than three spliced and unspliced transcripts were removed by filtering; thus, the final merged dataset comprised 28,952 genes and 119,062 cells.

The total mRNA counts were scaled by library size factors and log_{1p}-normalized, while protein counts were normalized via a centered log ratio transformation across each gene. Four thousand highly variable genes (HVGs) were identified using a local polynomial regression between the log of expression variance and the log of mean expression as implemented in the FindVariableFeatures function. After scaling the normalized counts, 100 principal components were computed using the set of HVGs as input, and

each cell was scored and assigned a cell cycle phase as described previously (35). Next, the 25 different samples were integrated by the Harmony package v0.1.1, which corrects the existing Principal Component Analysis (PCA) embedding (36). The first 50 principle components were used as input, and a two-dimensional UMAP embedding was computed using the cosine distance on the resulting 50 Harmony components (37). Lastly, an approximate shared nearest neighbors graph was computed on the first 50 Harmony components using the cosine distance with the number of nearest neighbors set to 100, and the resulting graph was partitioned into clusters via Louvain modularity optimization using a resolution of 0.1 (38).

2.3.3 scRNA-seq annotation

After clustering, the SingleR package v2.0.0 was used with several different immune reference datasets with known labels to assign a most-likely broad cell type to each cluster (39–44). In addition, the Azimuth package was used to map reference labels from an annotated dataset of healthy human PBMCs to each cell at multiple levels of granularity (34). Lastly, between-cluster differential expression testing was performed using the Wilcoxon rank-sum test with *p*-values adjusted via the Bonferroni correction. Genes were considered for testing if they were expressed by at least 25% of the cells in the cluster being tested, and results were retained if the mean log₂ fold-change was greater than 0.25 and the adjusted *p*-value was less than 0.05 (45, 46). After a comparison of the resulting differentially expressed gene sets (DEGs) with canonical marker genes from the literature and an investigation of the unsupervised annotations, a broad cell type identity was manually assigned to each cluster.

After subsetting the initial dataset to just the cluster labeled as monocytes, cells with confident T-cell labels from Azimuth were filtered out and the data were split into two groups based on whether the cells came from healthy subjects or septic patients. Subcluster analysis was performed on the monocytes from the healthy subjects and septic patients. Briefly, the data were reprocessed and reintegrated as described before, though the number of HVGs was lowered to 3,000 and only 30 principal components were used as input to the integration, nonlinear dimension reduction, and clustering routines. In addition, the number of estimated nearest neighbors was reduced based on the smaller sizes of the subsets. Any further subclustering of heterogeneous cell types was performed using the same methods. Differential expression testing was again used to identify potential marker gene sets, and a fine cell type label was manually assigned to each cluster. Lastly, the cell type labels were subjected to confirmatory analysis using the available cell surface protein data as needed.

2.3.4 scRNA-seq differential expression

Differential expression testing between for each time point versus healthy subjects in the “classically” annotated MDSCs was performed using a pseudobulk approach. Counts across all cells for each patient were aggregated and summed, then the DESeq2 method was applied for differential testing using the muscat R package v1.14.0 (47). The cell-type specific marker gene expression testing on the MDSCs annotated using the “emergent” view was performed using the FindAllMarkers function in Seurat using the Wilcoxon test.

Differentially expressed testing between sepsis groups was performed using linear mixed models. Each gene was tested between comparison groups for M-MDSCs, as they were the only population of MDSCs with a sufficient number of cells ($n > 50$) per group. Normalized expression was used as the response, with a binary indicator for sepsis group as the sole fixed effect. A random intercept was included for each sample, and models were fit via the maximum likelihood estimation using the `MixedModels.jl` Julia package (48, 49). After recording expression statistics such as mean expression per group, raw fold change, and log₂ fold change, the p -value of the group difference fixed effect from the linear mixed model was used to determine the significance of differential expression after adjustment using the Holm correction (38, 50).

2.3.5 Enrichment of genes with high transcriptional activity in MDSCs

The unspliced ratio per gene per cell was calculated as (unspliced counts + 1) divided by the (spliced counts + 1), then the mean for each gene was calculated separately for the MDSC subpopulations. Genes having a mean ratio greater than 1.1 were considered as having a high degree of active transcription. The `gprofiler2` R package v0.2.1 (51) was used to identify significantly enriched biological processes for each set of genes, then a network-based approach was performed to better understand biological functions using the `vissE` R package v1.8.0 (52). Similarities among the enriched processes were computed using the Jaccard index and then used to build an overlap network. Clusters of enriched gene-sets were identified by graph clustering; for each cluster a frequency analysis of words in the gene-set names indicates the most relevant biological functions.

2.3.6 scRNA-seq trajectory inference and RNA velocity

After annotating the septic monocytic cells, the data were further subject to only include the cell types thought to be relevant to MDSC development and differentiation: classical and non-classical monocytes, conventional dendritic cells (cDCs), and MDSCs. This subset was re-embedded using UMAP, and the cells were reclustered using the re-computed simulated neural network graph as input to the Louvain algorithm (37). After extracting the UMAP parameters from the output of the `RunUMAP` function, we used the `uwot` R package to regenerate the fitted UMAP model and nearest neighbor data that were generated internally (53). From this output we extracted the UMAP connectivity graph, which is a sparse representation of the fuzzy simplicial data set that can be loosely interpreted as a metric of how likely connections are between cells (37). The raw counts matrices, metadata for cells and genes, nearest neighbor graphs, PCA, Harmony, UMAP embeddings, and the UMAP connectivity graph were used to generate an `AnnData` object in Python that exactly matched the preprocessing used when annotating the cells in R (54).

The preprocessed data were used as input to an RNA velocity estimation workflow built around the `scVelo` package v0.2.5. After computing first-order moments of the spliced and unspliced counts,

the dynamical velocity model was used to estimate per-gene velocities and a cell-level velocity graph, after which the velocities were projected onto the existing UMAP embedding (55, 56). Next, transition probability matrices, absorption probabilities, and initial and terminal cell state likelihoods were estimated based on a weighted kernel of the velocity estimates and UMAP connectivities using the `CellRank` package v1.5.1 (57). The resulting cell fate probabilities then served as a prior for the estimation of a gene-shared latent time for each cell. Lineage driving genes were identified by estimating the Spearman correlation of each gene's expression with absorption probabilities for each identified cell fate. Finally, a directed partitioned graph abstraction was estimated and projected into the existing UMAP embedding using the state probability and latent time estimates as priors; these computations were performed using the partition-based graph abstraction (PAGA) algorithm as implemented in v1.9.3 of the `Scanpy` package (58, 59). In addition, an undirected graph abstraction was used as the initialization for a force-directed graph embedding of the cells, after which the graph abstraction was recomputed on the resulting embedding. This layout of the cells was used to display inter-cell type connectivities, which were estimated as described previously using UMAP (60, 61).

Differences in the dynamical model parameters (state probabilities, velocity length and pseudotime, cell stability index, and lineage priming) were tested between septic groups within MDSC subpopulations using a linear mixed model. Specifically, the `nlme` R package v3.1-162 (62) was used to fit a model with fixed effects of cell type, group, their interaction, and a random intercept for subject. Pairwise testing was then obtained using contrasts of interest (across groups within cell type) with the `emmeans` R package v1.8.7 (63).

2.3.7 Determination of sample size adequacy for assays

For estimating power for scRNA-seq, assuming detection of 10% in the proportion of MDSCs between cohorts with a 4% standard deviation, at least 4 subjects are required in each group to reach 90% power using a two sample t-test at the two-tailed 5% alpha level. This was established on the pilot study (64). Considering flow cytometry, this was not an endpoint of our analysis and therefore we reviewed available data at the onset of the study in order to determine gating for our cell subpopulation proportions. A power analysis was not conducted. Regarding T-cell proliferation and T-cell cytokine supernatant production, using a minimum of $n=8$ per group, assuming a difference of means of 26 with standard deviation 14 (based on prior data from similar assays) achieves 93% power based on a two sample t-test at the two-tailed 5% alpha level.

3 Results

3.1 MDSC subpopulations initially defined by classical cell surface markers

We used CITE-seq to analyze single-cell transcriptomic profiles of MDSCs in blood from healthy subjects ($n=12$) and surgical sepsis

patients at 4 ± 1 (n=4) and 14-21 (n=9) days after sepsis onset (65). Septic patients at 14-21 days were further divided based on their clinical outcomes at time of sampling, defined as either ‘rapid recovery’ (n=4) or development of CCI (n=5). Sex, age, and BMI were similar between cohorts (Table 1).

Similar to flow cytometry phenotyping, CITE-seq employs conventional cell surface markers for myeloid cell subpopulations to define E-MDSCs ($\text{Lin}^- \text{HLADR}^{\text{low/-}} \text{CD33}^+ \text{CD11b}^+ \text{CD14}^- \text{CD15}^- \text{CD66b}^-$), PMN-MDSCs ($\text{Lin}^- \text{CD33}^+ \text{CD11b}^+ \text{CD14}^-$ and CD15^+ or CD66b^+), and M-MDSCs ($\text{Lin}^- \text{HLADR}^{\text{low/-}} \text{CD33}^+ \text{CD11b}^+ \text{CD14}^+ \text{CD15}^- \text{CD66b}^-$), as well as $\text{CD14}^+ \text{CD16}^-$ (classical) and $\text{CD14}^{\text{dim}} \text{CD16}^+$ (non-classical) monocytes (while removing platelets, erythrocytes, HSPCs, $\gamma\delta$ T cells, and innate lymphoid cells). This is consistent with the classical monolithic view of myeloid differentiation described by Hegde (Figure 1A) (13). Historically, flow cytometry classification of MDSCs is performed directly on isolated PBMCs (4, 16) and our analysis revealed that PMN-MDSCs made up the majority of MDSCs in isolated PBMCs of representative septic patients, consistent with prior literature (Table 2) (4, 16).

We then evaluated cell proportions using transcriptomics with confirmation via flow cytometry. Myeloid cell enrichment was necessary in this step in order to detect MDSCs in healthy subject samples during CITE-seq as they are a relatively rare population (see Methods Section entitled “Human Blood Collection and Sample

Preparation”). Both single-cell transcriptomics and flow cytometry revealed an overall increase in total MDSCs acutely after sepsis (Figure 1B and Table 3). We plotted the cells via UMAP based on timepoint after sepsis (Figure 1C) and myeloid cell subtype (Figure 1D), which revealed heterogeneity of these cells when analyzing their single cell transcriptomes. The classification of MDSCs based on cell surface phenotypes is somewhat dependent on the method of analysis, and as the myeloid enrichment kit (STEMCELL) uses CD33 (and CD33 is expressed on all MDSCs), this was our first inclination that an alternative method of classifying cells by subpopulation would be necessary.

Next, we performed pseudobulk differential gene expression between septic patients at day 4 and days 14-21 post-sepsis diagnosis compared to healthy subjects to assess possible differences among septic groups. Dramatic differences in gene expression within MDSC subpopulations (specifically PMN- and M-MDSCs, which were most abundant) were observed that varied over time (Figure 2). Considering PMN-MDSCs, by comparing each differential expression test performed against healthy subjects, we found more extreme fold-changes in late sepsis patients who developed CCI compared to acutely septic patients (Figure 2A, left panel). Conversely, gene expression for late sepsis patients who rapidly recovered returned towards that seen in healthy subjects when compared to both acute sepsis and late sepsis with CCI. Gene expression for rapid recovery and CCI patients compared to healthy

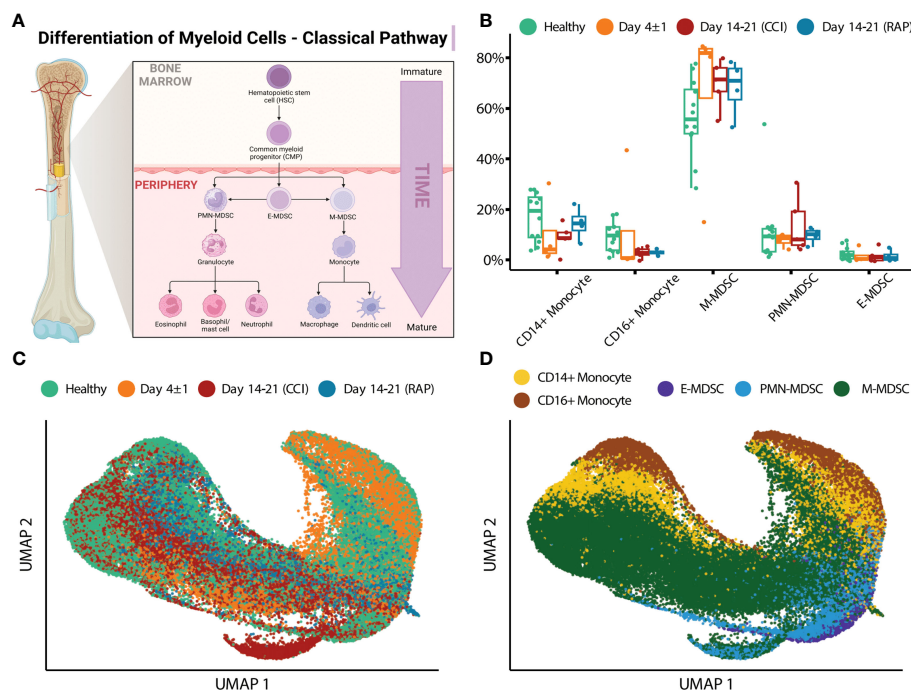


FIGURE 1

Single-cell analysis of myeloid cells using surface protein markers. (A) Illustration representing the historical/classic/monolithic definition of MDSCs. E-, PMN-, and M-MDSCs are the predominant subpopulations with distinct phenotypes and functions (modified from Hegde et al. (13)). Created with BioRender.com. (B) Cell proportions of monocyte subtypes and MDSCs relative to overall monocytic cells are shown for healthy subjects (“Healthy”) (n=12), septic patients 4 days following diagnosis (“Day 4 ± 1 ”) (n=4), and septic patients at days 14-21 (separated into those experiencing chronic critical illness (“CCI”) (n=5) or those who rapidly recovered (“RAP”) (n=4)). (C) UMAP embedding of single-cell transcriptomes of peripheral blood mononuclear cells (PBMCs). Cells are colored by the timepoint at which the samples were taken. Samples from day 4 and days 14-21 are from septic patients. (D) Similar to (C), with cells colored by cell type. M, monocytic; PMN, granulocytic; E, early.

TABLE 2 Percentage of total MDSCs and MDSC subpopulations from PBMCs via flow cytometry.

MDSC Subpopulation	Healthy Subjects (n=6)	Sepsis Day 4 ± 1 (n=7)	Sepsis Days 14-21 (n=3)
% Total MDSCs	15.1 (8.1, 16.6)	39.2 (25.2, 55.6)	44.8 (35.6, 56.3)
% E-MDSC	68.1 (49.8, 78.7)	1.4 (0.7, 5.9)	2.3 (2.2, 9.0)
% PMN-MDSC	14.6 (7.4, 36.9)	79.5 (64.4, 89.0)	80.7 (52.0, 85.1)
% M-MDSC	9.2 (4.9, 12.7)	9.1 (8.1, 12.7)	11.5 (9.7, 35.9)
% Ungated	2.0 (1.4, 3.2)	0.7 (0.5, 1.3)	0.7 (0.7, 3.1)

Percentages of MDSC populations in representative septic patients. Blood was collected from healthy subjects (n=6), day 4 ± 1 septic patients (n=7), and late sepsis patients at days 14-21 (n=3). PBMCs were isolated and prepared for flow cytometry. Viable cells determined followed by gating of CD11b⁺ and CD33⁺ cells. HLA-DR^{low} cells selected to capture total MDSCs. CD11b⁺ CD33⁺ HLA-DR^{low} cells outside the gating of the three MDSC subpopulations are classified as “% Ungated.” Results reported as median (Q1, Q3). E, early; PMN, granulocytic; M, monocytic.

subjects also tended to diverge (Figure 2A, middle and right panels). Overall, 52 genes were differentially expressed in PMN-MDSCs from acutely septic patients; however, only three of these genes were also significantly differentially expressed in patients who rapidly recovered and those who developed CCI (Figure 2B; Supplementary File 1). The ontology of transcriptional differences among septic patients at different time points also illustrated the heterogeneity of the PMN-MDSC response over time (Figure 2C).

The greatest differences in the magnitude of M-MDSC gene expression from healthy subjects compared to septic patients occurred during acute sepsis (Figure 2D). In this cohort, 601 genes were differentially expressed in M-MDSCs, and only 31 of these were also significantly differentially expressed in late sepsis patients who rapidly recovered and those who developed CCI (Figure 2E). Gene ontology analysis among M-MDSCs revealed that patients experiencing rapid recovery had over-expression of

TABLE 3 Percentage of total MDSCs and MDSC subpopulations from PBMCs and enriched myeloid cells via flow cytometry.

MDSC Subpopulation	Healthy Subjects (n=9)	Sepsis Day 4 ± 1 (n=3)	Sepsis Days 14-21 (n=6)
% Total MDSCs	0.3 (0.1, 0.3)	3.1 (1.8, 3.6)	0.8 (0.5, 1.3)
% E-MDSC	1.3 (1.1, 5.3)	0.7 (0.5, 1.2)	1.0 (0.5, 6.0)
% PMN-MDSC	22.9 (11.6, 30.3)	26.7 (16.5, 34.5)	23.5 (16.0, 39.9)
% M-MDSC	67.1 (64.6, 83.1)	71.0 (64.0, 81.4)	68.2 (57.2, 80.6)
% Ungated	0.3 (0.0, 0.5)	0.6 (0.3, 1.6)	0.5 (0.3, 0.7)

Percentages of MDSC populations in representative septic patients. Peripheral blood mononuclear cells and myeloid cells were collected from the same septic cohorts (n=3 for acute sepsis and n=6 for late sepsis patients) and healthy subjects (n=9). A 3:1 mixture of myeloid cells: enriched PBMCs were prepared for flow cytometry. Cells outside the gating of the three MDSC subpopulations are classified as “% Ungated.” Results reported as median (Q1, Q3). E, early; PMN, granulocytic; M, monocytic.

kinase agents versus oxoacid metabolism when compared to sepsis patients with CCI (Figure 2F).

In summary, transcriptomic analysis comparing healthy subjects, patients day 4 post-sepsis, and patients at days 14-21 post-sepsis (combining those who rapidly recovered with those who developed CCI) revealed significant heterogeneity in MDSC transcriptomics. In addition, lymphocyte suppressive activity, specifically suppression of T cell proliferation and T cell cytokine/chemokine production, varied between cohorts (see below). MDSCs from both time points after sepsis were dissimilar when comparing their gene expression profiles and significantly enriched biological processes from gene ontology.

3.2 Verifying the immunosuppressive capacity of MDSCs present in sepsis

Our laboratory has previously used cell sorting and subsequent T-cell suppression assays to demonstrate the immunosuppressive capacity of total MDSCs from septic patients (4, 16). Thus, we set out to verify that functionally active PMN- and M-MDSCs were indeed present in the isolated PBMCs of septic individuals, as defined by Gabrilovich et al. (11). Surprisingly, we discovered unexpected cell types in our flow cytometry samples that were supported by single-cell analysis. Historically in the cancer literature, CD15 positivity is used to distinguish PMN-MDSCs from M-MDSCs (13). However, in representative septic patients, after identifying CD11b⁺CD33⁺ cells (Figure S1A) and isolating HLA-DR^{low} cells to obtain the total MDSC population (Figure S1B), CD15 was unable to clearly separate MDSC subpopulations (Figure S1C, bottom panel). Alternatively, CD66b (CEACAM8; a granulocytic marker) was able to better delineate MDSC subpopulations (Figure S1C, top panel) and, thus, was selected to distinguish PMN-MDSCs from PBMCs for functional analysis (Figure S1D) (10, 11, 19, 20, 66). We undertook bulk CD66b⁺ cell isolation (STEMCELL Technologies, Vancouver); however, although CD14⁺CD15⁺ PMN-MDSCs enrichment was achieved, further analysis of the CD66b⁺-isolated cells demonstrated distinct CD66b^{low} and CD66b^{high} populations (Figure S2A). Thus, we had enriched CD66b^{low}CD14⁺CD15⁻ M-MDSCs in our gating strategy which was meant to only contain PMN-MDSCs (CD66b^{high}) (Figure S2B).

Functionally, the CD66b⁺ cells isolated from septic patient PBMCs suppressed either CD4⁺/CD8⁺ T-lymphocyte cytokine/chemokine production (Figure S3) or lymphocyte proliferation of host CD8⁺ T-lymphocytes (Figure S4), thereby meeting the criteria of MDSCs. CD66b⁺ MDSCs from septic but not healthy subjects altered T-cell cytokine production in response to anti-CD3/CD28 treatment, including IFN- γ , IL-2, IL-4, IL-10, and IL-17 (Figure S3). Cytokines which were analyzed which did not exhibit CD66b⁺ inhibition in acutely septic patients include IL-12, IL-23, and TGF- β . CD66b⁺ cells isolated from sepsis patients 14-21 days after infection were capable of significantly suppressing CD8⁺ T-lymphocyte proliferation in response to CD3/CD28 stimulation (Figure S4). Although we did not see suppression of CD4⁺ T lymphocyte proliferation by CD66b⁺ cells, we did see a

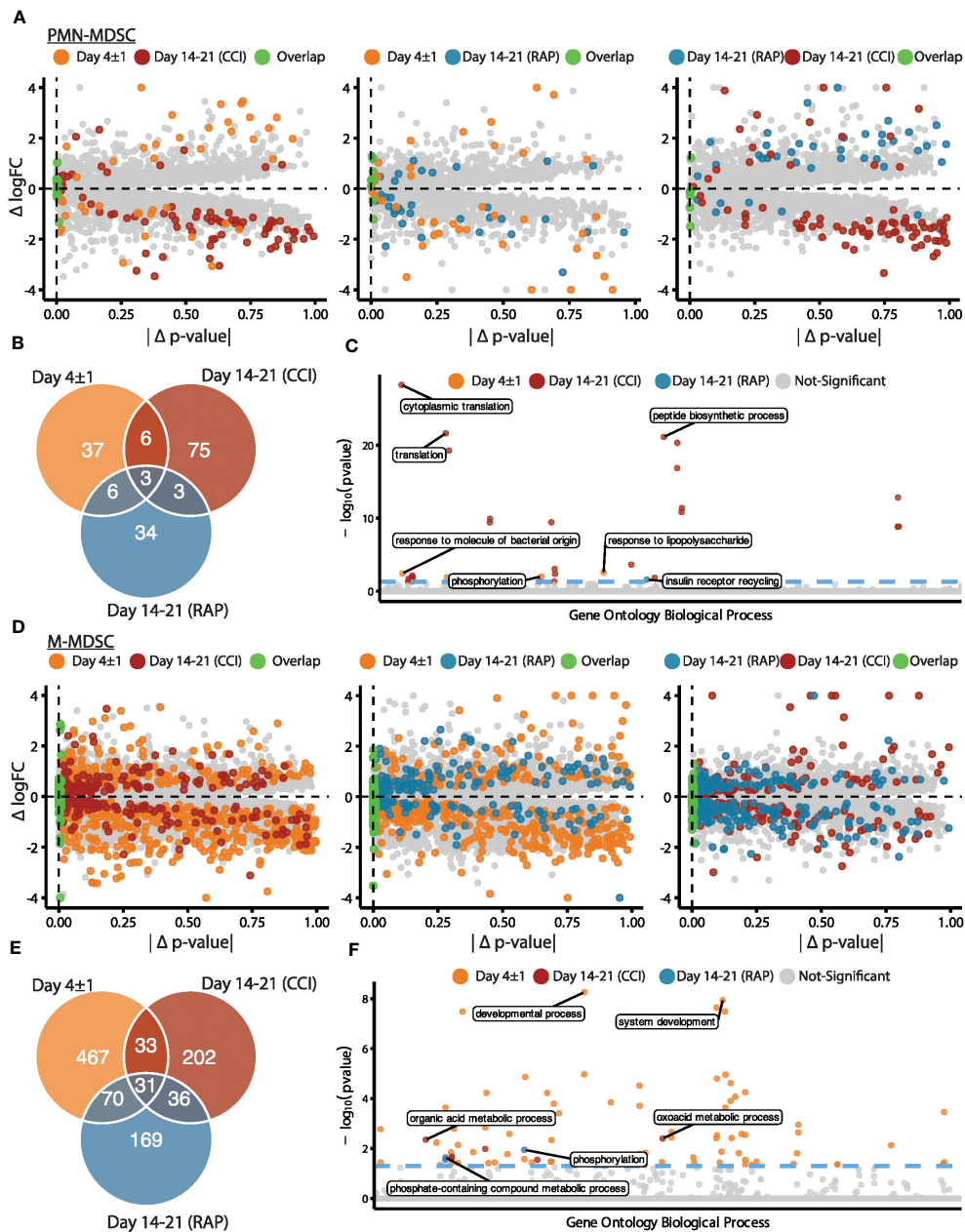


FIGURE 2

Analysis via CITE-seq of differential gene expression of PMN- and M-MDSC subpopulations at different time points relative to healthy subjects. (A) Within PMN-MDSCs, gene expression of twelve healthy subjects (baseline) was compared with septic patients at day 4 ("Day 4 ± 1") (n=4) and septic patients at days 14-21 (subdivided into chronic critical illness ("CCI") (n=5) and rapid recovery ("RAP") (n=4)). Differential expression results relative to healthy subjects were compared for each pair of septic time points (left panel: day 4 vs CCI, middle panel: day 4 vs RAP, right panel: RAP vs CCI). The x-axis is the absolute difference in the p-value per gene ($|\Delta p\text{-value}|$) and the y-axis is the difference in log fold-change ($\Delta \log\text{FC}$). The colored points represent genes that were differentially expressed in a single group or for both groups ($p\text{-value} < 0.01$). (B) Venn diagram of genes with overlapping significant differential expression ($p\text{-value} < 0.01$). (C) Enrichment results of significant genes representing the gene ontology biological processes. The y-axis is the negative log (base 10) of the p-value ($-\log_{10}(p\text{value})$). (D-F) Similar to (A-C) for M-MDSCs. PMN, granulocytic; M, monocytic.

significant decrease in stimulated T-lymphocyte production of IFN-gamma at days 14-21 compared to day 4 (Figure S5). This indicates that T lymphocytes are incapable of maintaining IFN-gamma production 2-3 weeks after sepsis (similar to what has been previously reported) (67), and that MDSCs at this time point may not be able to further suppress this aspect of CD4+ T lymphocyte function (22, 67).

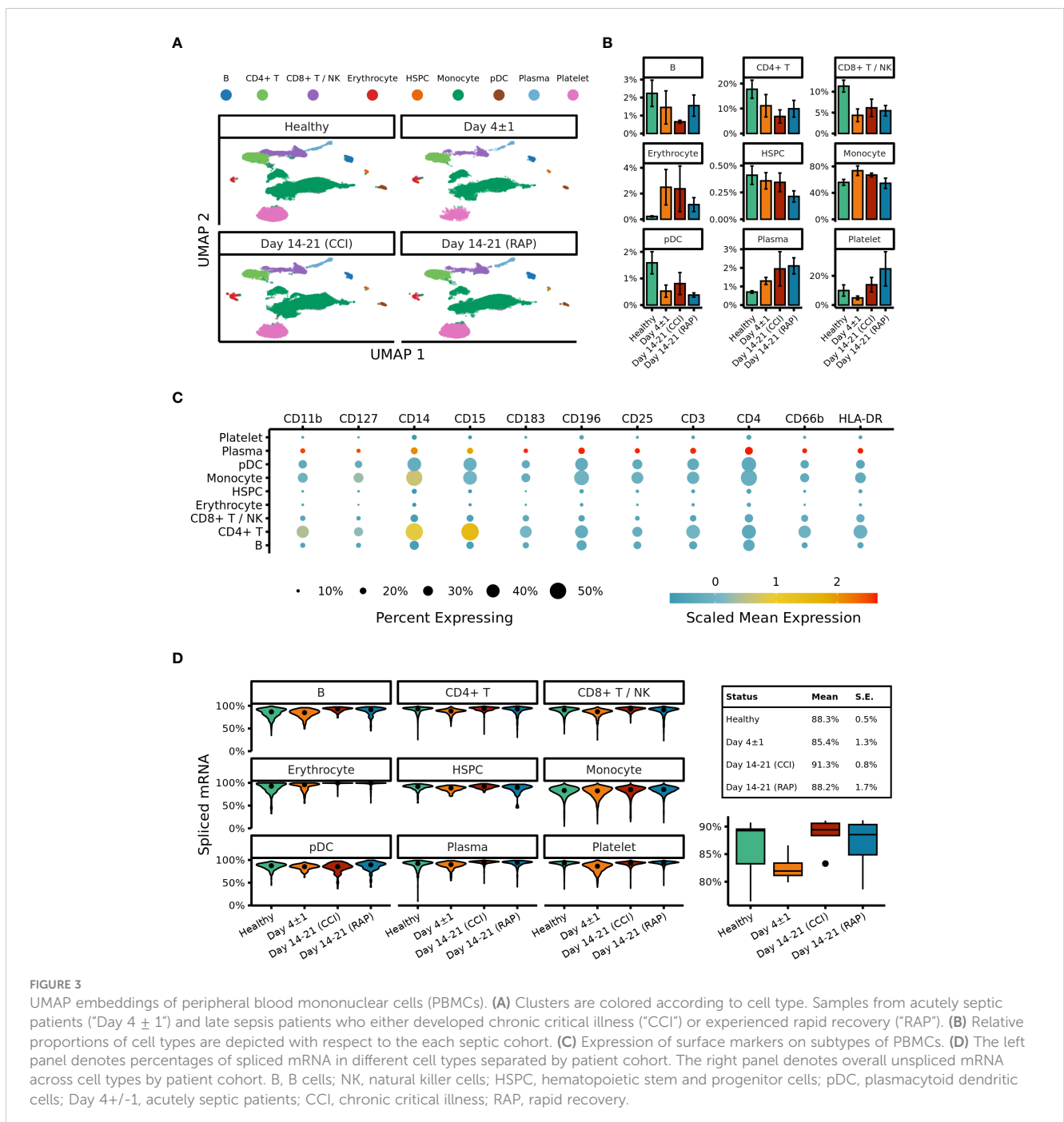
3.3 Emergent view of MDSCs and transcriptomic analysis of a novel MDSC subpopulation

After our initial steps demonstrated that identification of MDSC subsets based on cell surface markers was potentially problematic in sepsis, we transitioned to cell classification via gene expression for

the remainder of our analysis. All cells were clustered based on their transcriptomic profiles (visualized via UMAP (Figure 3A) with relative percentages of each cell type depicted in Figure 3B). The broad cell types were compared via expression of cell-surface marker genes (Figure 3C) as well as percentage of spliced mRNA between patient groups (Figure 3D). This was followed by careful manual annotation and inspection of canonical marker genes with identification of myeloid cells via differential expression of genes (Figure 4). As explained by Hegde et al. (13), there is substantial plasticity within MDSC subpopulations during sepsis which informs the relationship between MDSCs and terminally

differentiated effector cells (Figure 5A). Additional marker genes were used to obtain fine-level annotation of myeloid cell types (Figure 5B). Importantly, four distinct populations of MDSCs were identified via this approach (Figure 5C), three of which were consistent with classically defined E-, PMN-, and M-MDSCs (11).

A novel fourth population was identified in 60% of the late sepsis patients who developed CCI, as well as both of the acutely septic patients who progressed to CCI (Table 4, Figure 6A). This MDSC subpopulation exhibited gene expression patterns that were partially consistent with both M- and PMN-MDSCs. We thus labeled these cells “hybrid” (H)-MDSCs. Although one of the



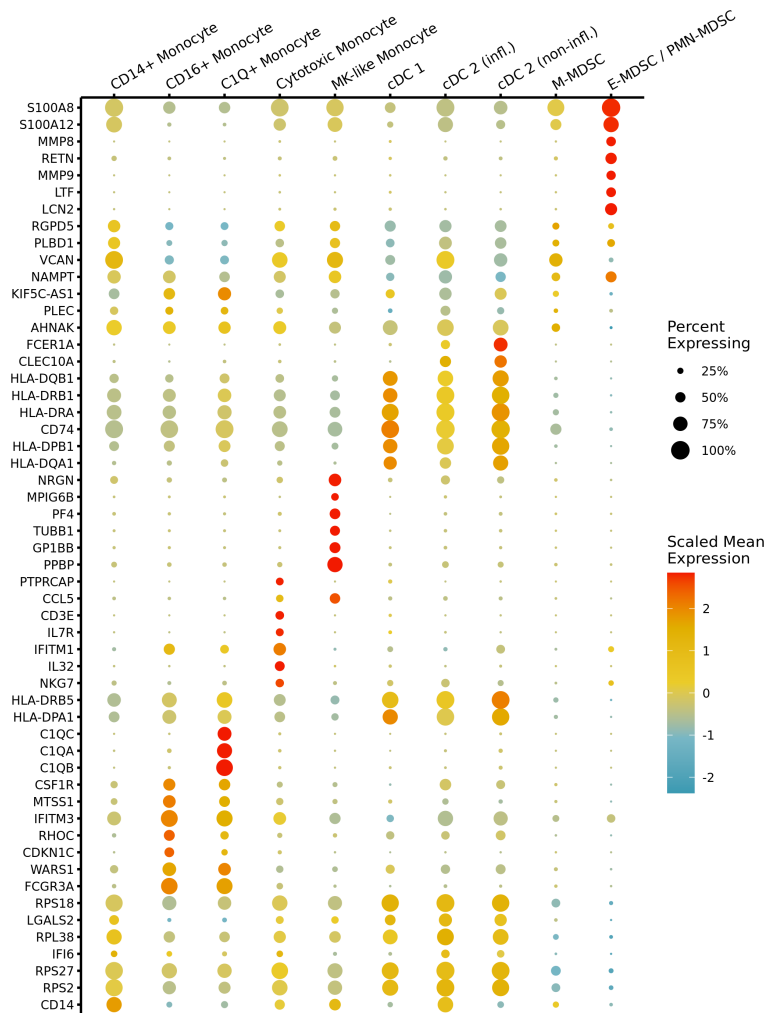


FIGURE 4

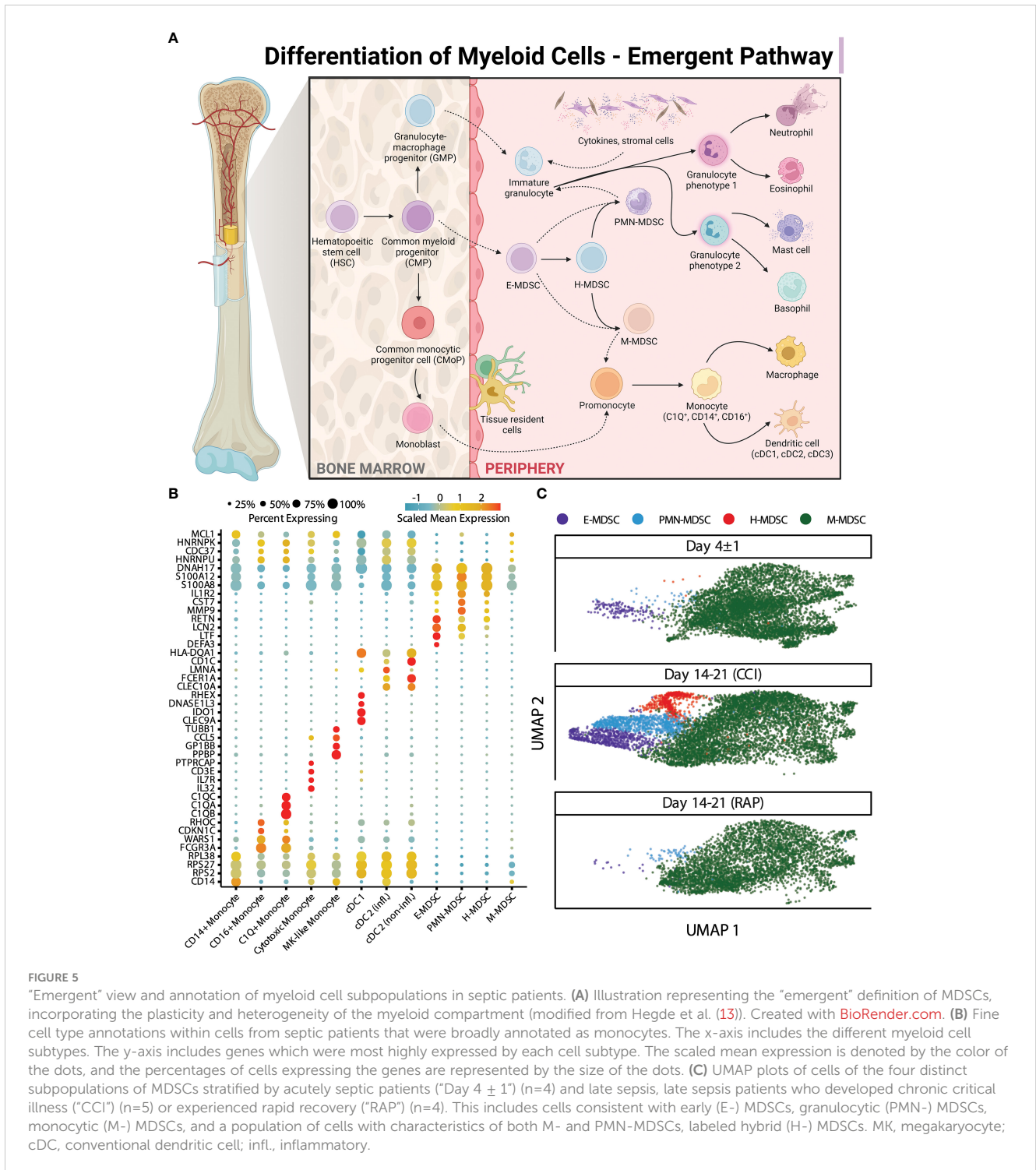
Marker gene expression across myeloid cell types in septic patients. A dot plot shows scaled mean expression of the top seven most significant differentially expressed genes (DEGs) in each myeloid cell type prior to fine-level annotation for MDSC subpopulations. Point radius indicates the percentage of cells with nonzero expression, and color denotes relatively higher or lower mean expression across cell types. Testing was performed with the Wilcoxon test, and genes were ranked by adj. *p*-value after Bonferroni correction. CD14⁺: classical monocyte, CD16⁺: non-classical monocyte, MK, megakaryocyte; cDC, conventional dendritic cells; infl., inflammatory; M, monocytic; E, early; PMN, granulocytic.

patients with CCI had a much greater number of H-MDSCs than other patients, it should be noted no H-MDSCs were observed in late sepsis patients who had rapidly recovered, or acutely septic patients who progressed to rapid recovery (Table 4). One of our acutely septic patients died within 14 days, giving us an acute sepsis mortality rate of 25%. This is similar to previously reported literature in septic ICU patients (68). The patient that experienced an early death had similar proportions of MDSC subpopulations compared to the other acutely septic patients (M-MDSCs: 61% vs 51 ± 13%, PMN-MDSCs: 0.2% vs 0.7 ± 0.6%, E-MDSCs: 0.08% vs 2 ± 3%, H: 0% vs 0.2 ± 0.5%).

The majority of MDSC-specific genes in septic patients were shared by at least two of the four subpopulations (66%, *n*=270 genes), with 36% (*n*=147 genes) significantly expressed by all four (Figure 6B, Supplementary File 2). Although the MDSC subpopulations were fairly similar in terms of overlapping genetic expression, we identified seven genes uniquely expressed by H-

MDSCs: *RGDP5*, *TBL1X*, *MBNL1*, *SERF2*, *ATP5F1E*, *MT-ND1*, and *MT-ATP6* (Figure 6C). Gene expression was downregulated in RANBP2-like and GRIP domain-containing protein 5 (*RGDP5*), transducin (beta)-like 1X-linked (*TBL1X*), and muscleblind-like splicing regulator 1 (*MBNL1*) (69, 70). *TBL1X* regulates transcriptomic pathways and is upregulated in malignancy (69). *MBNL1* regulates alternative splicing and can be up- or downregulated depending on the type of cancer (71). Genes with upregulated expression included small EDRK-rich factor 2 (*SERF2*), ATP synthase F1 subunit epsilon (*ATP5F1E*), NADH-ubiquinone oxidoreductase chain 1 (*MT-ND1*), and mitochondrially encoded ATP synthase membrane subunit 6 (*MT-ATP6*). The latter three genes encode proteins involved in mitochondrial metabolism and function (72).

We next sought to identify differential genetic expression between our septic cohorts, specifically looking at differences between MDSCs in late sepsis patients who rapidly recovered



compared to those who developed CCI. For differential expression across sepsis groups, only M-MDSCs were sufficiently present per group for fitting a linear mixed model with multiple subjects, as MDSCs are a relatively rare population overall. We identified four differentially expressed genes in M-MDSCs using this method: *CD163*, *IER2*, *CTSZ*, and *SNX3* (Figure 6D). Expression of *CD163* (73), a gene responsible for controlling inflammation, was significantly lower in M-MDSCs in late sepsis patients with CCI versus acutely septic patients. *SNX3*

has been identified as a potential septic biomarker (74), and was significantly upregulated in patients with CCI compared to acutely septic patients. *IER2* was significantly higher expressed in late sepsis patients who rapidly recovered compared to acutely septic patients. *IER2* is known to be upregulated in response to external stimuli including infection (75, 76). *CTSZ* expression was significantly higher in patients with CCI compared to patients who rapidly recovered after sepsis, and has been previously identified as a septic marker in mice (77).

TABLE 4 H-MDSC cell counts by patient and associated outcome after sepsis.

Patient #	Patient Classification	Eventual classification if acute sepsis	H-MDSC Cell Counts
1	Acute Sepsis	Early death	0
2	Acute Sepsis	Rapid recovery	0
3	Acute Sepsis	CCI	1
4	Acute Sepsis	CCI	8
5	Rapid recovery		0
6	Rapid recovery		0
7	Rapid recovery		0
8	Rapid recovery		0
9	CCI		552
10	CCI		6
11	CCI		1
12	CCI		0
13	CCI		0

H-MDSC cell counts as determined by manual annotation. If blood samples were taken from acutely septic patients at day 4, then their eventual sepsis classification has been recorded. H, hybrid; CCI, chronic critical illness.

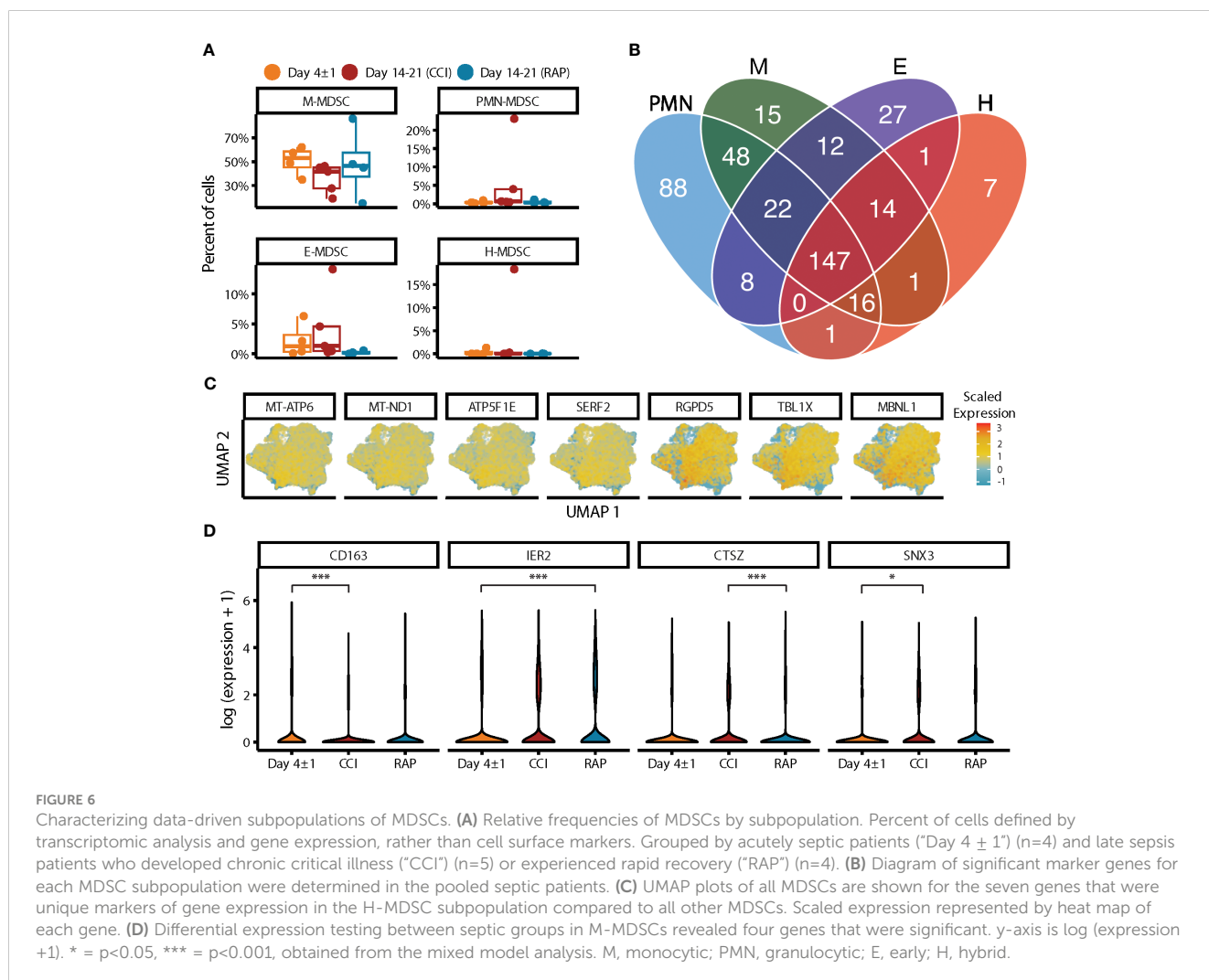


FIGURE 6

Characterizing data-driven subpopulations of MDSCs. **(A)** Relative frequencies of MDSCs by subpopulation. Percent of cells defined by transcriptomic analysis and gene expression, rather than cell surface markers. Grouped by acutely septic patients ("Day 4 ± 1") (n=4) and late sepsis patients who developed chronic critical illness ("CCI") (n=5) or experienced rapid recovery ("RAP") (n=4). **(B)** Diagram of significant marker genes for each MDSC subpopulation were determined in the pooled septic patients. **(C)** UMAP plots of all MDSCs are shown for the seven genes that were unique markers of gene expression in the H-MDSC subpopulation compared to all other MDSCs. Scaled expression represented by heat map of each gene. **(D)** Differential expression testing between septic groups in M-MDSCs revealed four genes that were significant. y-axis is log (expression + 1). * = p<0.05, *** = p<0.001, obtained from the mixed model analysis. M, monocytic; PMN, granulocytic; E, early; H, hybrid.

The plasticity of the H-MDSC subpopulation is evident in the increased per-cell proportion of unspliced mRNA, indicating more active transcription. Only E-MDSCs had a higher proportion of unspliced mRNA in the myeloid compartment (Figure 7A). To examine factors driving cellular activities, we identified genes with a high average proportion of unspliced mRNA within each cell subpopulation and performed enrichment analysis to identify

relevant biological processes. Rather than focusing on individual ontologies, we used a network-based approach to cluster similar significantly enriched biological functions for each MDSC subpopulation (Figures 7B-E) (52). Not surprisingly, actively transcribed genes in all MDSC subpopulations were enriched for activities pertaining to ‘immune activation.’ While PMN- and M-MDSCs had more biologically distinct functions, H-MDSCs shared

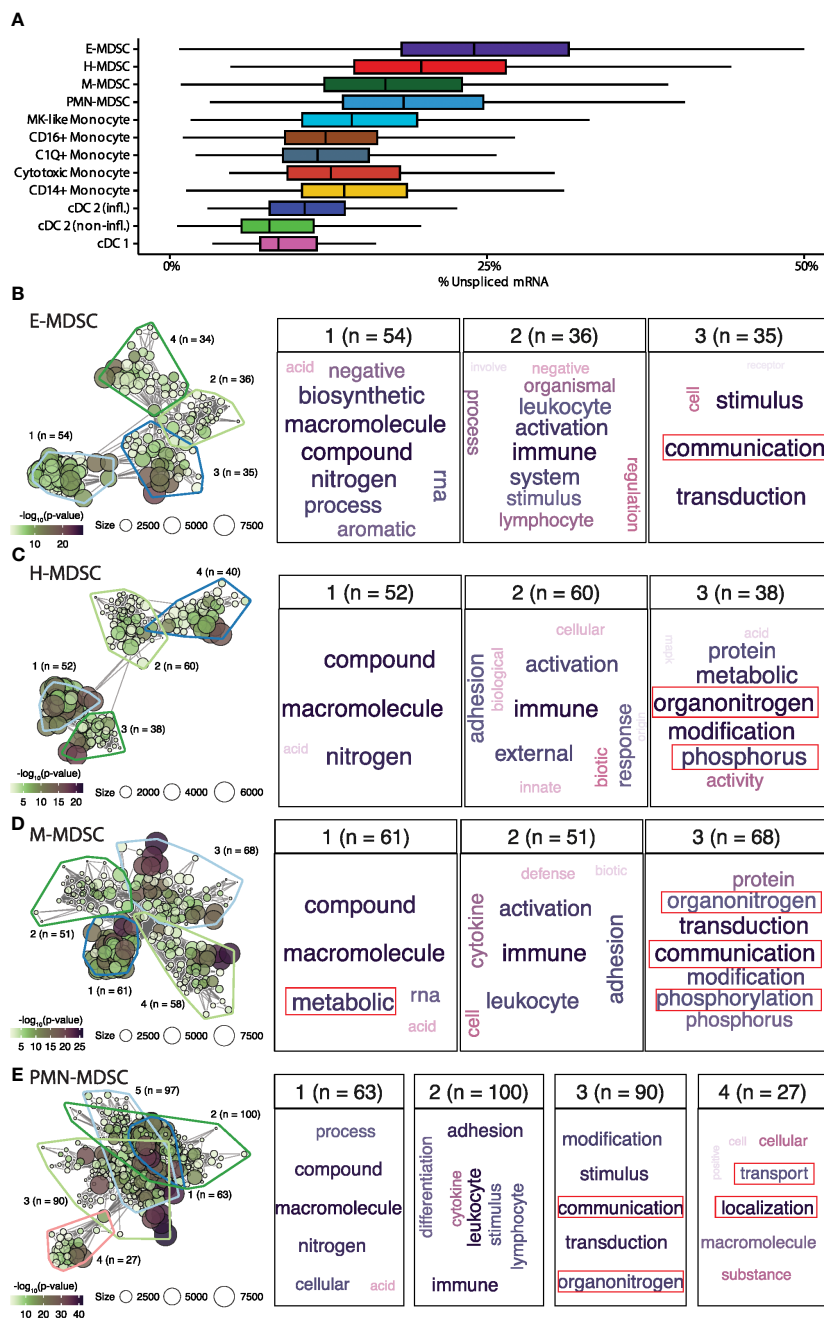


FIGURE 7 Larger proportions of unspliced mRNA in E- and H- MDSCs. **(A)** Distribution of unspliced mRNA percent across myeloid cell types. **(B-E)** Gene-set enrichment analysis of genes having high proportions of unspliced mRNA within each MDSC subpopulation. The left panel shows the gene-set network and clustering of significantly enriched biological processes. The right panels show word clouds for each biologically similar cluster (a general cluster of high-level biological processes was present for each cell-type and omitted). E, early; H, hybrid; M, monocytic; PMN, granulocytic; CD16⁺, non-classical monocyte; CD14⁺, classical monocyte; MK, megakaryocyte; cDC, conventional dendritic cell; infl., inflammatory.

enrichment with both cell types, specifically pertaining to pathophysiological septic-related processes including ‘organonitrogen’ and phosphorus-related processes.

3.4 Determination of differentiation pathways and cell lineage in septic cohorts

Having described the MDSC subpopulations, we next set out to incorporate these findings into differentiation pathways of the myeloid compartment in septic patients. Quantifying transcriptional kinetics via RNA velocity estimation revealed complex, fluid relationships between MDSC phenotypes (Figure 8A). As expected, M-MDSCs appeared to serve as the bridge between early immunosuppressive cell types and mature myeloid cells such as monocytes and cDCs (Figure 8B). As our analysis was based on PBMCs, it was not possible to compare the transition from MDSCs to mature granulocytes (PMNs). Estimating the graph connectivity between monocyte-lineage cell types allowed us to quantify the strength of each undirected relationship, and showed that MDSC subpopulations are both highly interconnected and much more internally similar to each other than they are to populations of terminally-differentiated myeloid cells (Figures 8B, C).

After analyzing velocity-inferred cell state transitions performed with CellRank, all E-, PMN-, and the vast majority of M-MDSCs cell states were classified as progenitor-like or transitioning-like (Figure 8D). Only H-MDSCs contained a significant proportion of cells in a plasticity-like state with high

probabilities for both initial and terminal cell states (in which cells remain H-MDSCs) (Figure 8E) (57). Supporting this, significant variation was observed in the likelihood of an H-MDSC staying an H-MDSC when estimated by absorption probabilities from CellRank, with a mean (SD) probability of 0.33 (0.29) (Figure 8F). No other cell types were likely to end up as H-MDSCs. To better characterize the biology underlying commitment to the H-MDSC cell fate, lineage driver genes (genes significantly correlated with the probability of becoming an H-MDSC) were identified by computing Spearman correlations of expression with absorption probabilities. Highly correlated genes were diverse in function and included inflammation-associated genes such as *S100A8*, *-9*, and *-12*, along with immunoregulatory genes *ALOX5A*, *RETN*, and *IL1R2*.

Next, we investigated differences in cell states across sepsis groups for each MDSC subpopulation. As H-MDSCs were not observed in sepsis patients who experienced rapid recovery, they were not included for this analysis. M-MDSCs were highly consistent between septic patients at day 4 and days 14-21 in terms of their cell states and kinetics (Figure 9A). Interestingly, PMN-MDSCs displayed the most heterogeneity, specifically in late sepsis patients with CCI compared to both day 4 septic patients and late sepsis patients who rapidly recovered. PMN-MDSCs in late sepsis patients who developed CCI had significantly slower differentiation speed, higher cell state stability, and lower initial state probabilities (Figure 9B). This is consistent with PMN-MDSCs persisting in CCI compared to patients who rapidly recover after sepsis. E-MDSCs in late sepsis patients with CCI also showed significantly lower differentiation progression than acutely septic patients or late sepsis patients who rapidly recovered, along with a

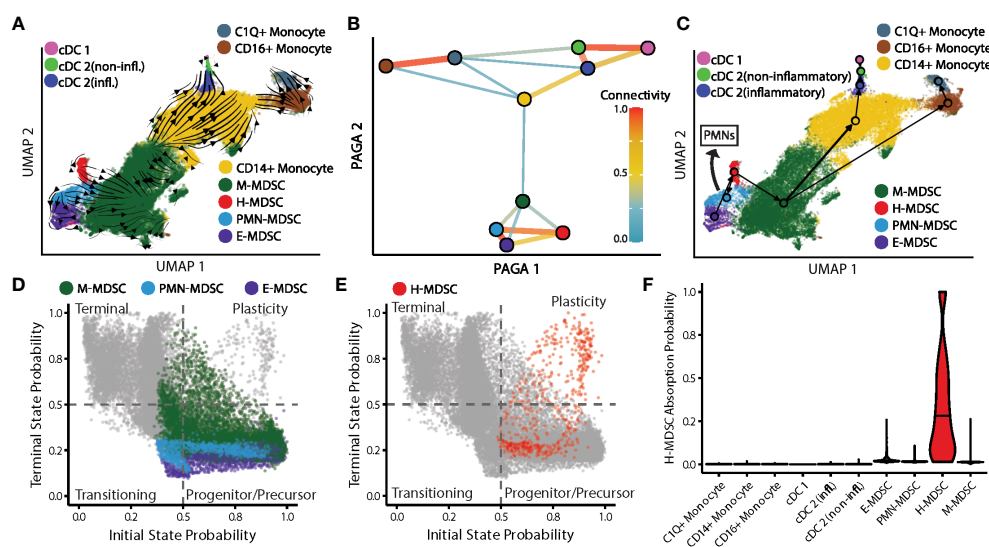


FIGURE 8

Topology of myeloid differentiation and plasticity in septic patients. (A) Myeloid cell smoothed RNA velocity estimates projected onto UMAP. Arrows represent differentiation potential. (B) Undirected partition-based graph abstraction (PAGA) of myeloid cell types. Line width/color between cell types denote relationship strength. Nodes colored by cell type. (C) Arrow directions represent differentiation potential. Arrow widths denote strength of connectivities between cell types. Arrow manually added indicating PMN-MDSC differentiation into granulocytes. (D) Cell state probabilities shown together for M-, PMN-, and E-MDSCs with all other cells in gray. (E) Similar to (D) with H-MDSCs in red. (F) H-MDSC cell fate absorption probabilities. cDC, conventional dendritic cell; infl., inflammatory; CD16⁺, non-classical monocyte; CD14⁺, classical monocyte; M, monocytic; H, hybrid; PMN, granulocytic; E, early.

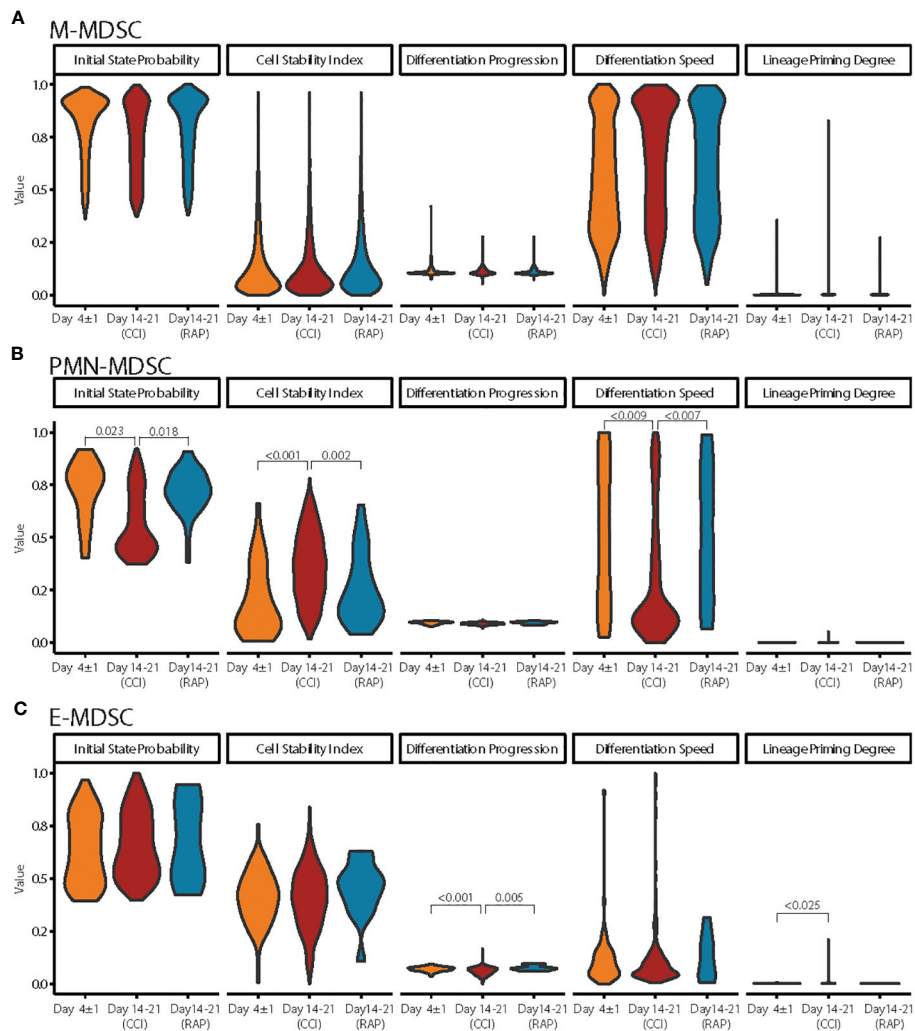


FIGURE 9

Differences in PMN-, E-, and M-MDSCs across septic time-points. (A) Cell dynamic parameters estimated from CellRank were compared across cells from septic patients at Day 4 ± 1 (acute sepsis) (n=4), patients at day 14-21 who rapidly recovered ("RAP") (n=4), and patients at day 14-21 who developed chronic critical illness ("CCI") (n=5) in M-MDSCs. (B, C) Similar to (A) for PMN-MDSCs and E-MDSCs, respectively. Significant *p*-values (< 0.05) were obtained from fitting a linear mixed model. E, early; PMN, granulocytic; H, hybrid; M, monocytic.

higher degree of cell commitment along the differentiation trajectory compared to acutely septic patients (Figure 9C).

As previously stated, CD66b⁺-isolated PBMCs met the criteria of MDSCs in their ability to suppress either T-lymphocyte cytokine/chemokine production or T-lymphocyte proliferation *ex vivo* (Figures 5, 6) (4, 16), although CD66b⁺-isolated PBMCs were not identical in their suppressive activity from acutely septic patients or late time periods after severe infection. Interestingly, whether using cell-surface markers or transcriptomic analysis of the current dataset, differential expression of several key MDSC genes published in the cancer literature did not reach significance and/or were modestly expressed in septic individuals (Figure 10). For example, although there was upregulation of genes in the *S100A* and *MMP* superfamilies, differential expression of *ARG1*, *IL-10*, *NOS2*, and *TGFBI* did not reach significance (although transcripts from all genes were detected).

4 Discussion

Since their delineation by Gabrilovich in 2007 (78), MDSCs have been reported in multiple inflammatory diseases in addition to cancer (79). Recently, Hedge et al. described significant heterogeneity among these immune suppressive cells in the myeloid compartment (13). They stated that historically we have had a 'monolithic view' or definition of MDSCs, and that a more complex 'emergent view' is required to better understand these leukocytes (13). In this report, we have taken both conceptual approaches (monolithic and emergent) to analyze MDSCs in one of the first cohorts to compare patients with poor (CCI) versus good (rapid recovery) clinical outcomes after surgical sepsis. Importantly, all analyses revealed significant alterations in the evolution of MDSCs after sepsis (i.e., time points) as well as significant differences in the MDSC subpopulations taken from sepsis

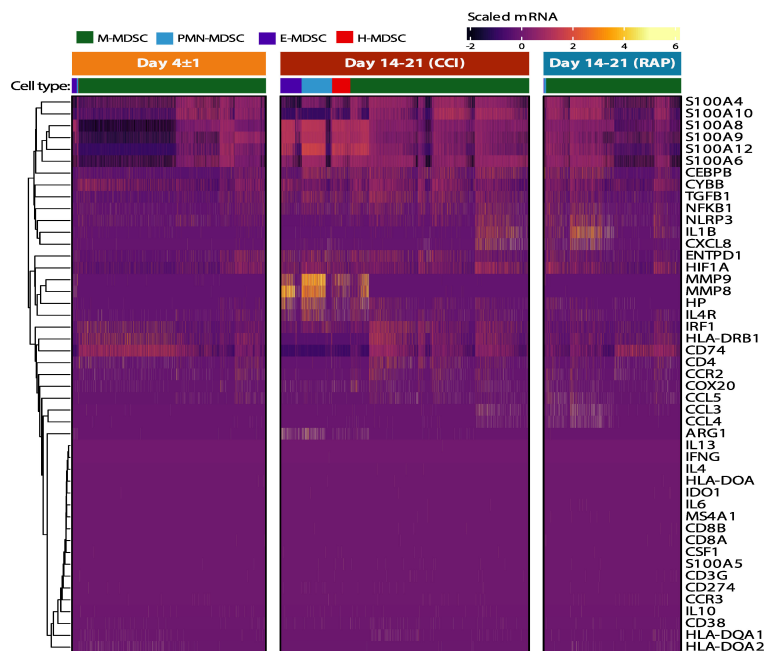


FIGURE 10

Canonical MDSC genes in immunosuppressive cell subpopulations in septic patients. Heatmap of scaled expression of canonical genes identified in the current MDSC literature. Cells in the four identified MDSC subpopulations are denoted in the colored key. Genes were arranged using hierarchical clustering with complete linkage. Patient groups include acutely septic patients ("Day 4 ± 1") (n=4) and late sepsis patients who developed chronic critical illness ("CCI") (n=5) or experienced rapid recovery ("RAP") (n=4). M, monocytic; PMN, granulocytic; E, early; H, hybrid.

survivors who rapidly recovered or developed CCI. In classifying MDSCs via gene expression and transcriptomic analysis, we have also identified a novel MDSC subpopulation (H-MDSCs) present only in sepsis survivors with CCI and acutely septic patients who progressed to CCI. Finally, even though we have demonstrated in this work and previously (16) that these cells suppressed lymphocyte proliferation to antigenic stimulation (similar to oncologic processes), the MDSCs identified after sepsis do not significantly express many of the well-described genes key to MDSC immunosuppression in other pathologies, most commonly cancer (80).

The study of MDSCs has expanded dramatically over the past decade. However, the overwhelming majority of these studies performed using blood samples are from cancer patients; only five studies focus on systemic infection and sepsis (8, 14, 81–83). Although MDSCs are commonly detected in different inflammatory pathologies, there is a gap in research regarding this cell type in the infected or post-infected host. Data are increasingly illustrating the impact of a dysregulated myeloid compartment in patients with poor long-term outcomes, including COVID-19 (84). MDSCs have been identified in these patients, especially those with more severe disease or poor outcomes (85, 86), and are being considered as a target for immunotherapy (87).

MDSCs are challenging to define and characterize. As such, cell surface markers and genes historically used to identify MDSC subpopulations were amassed from multiple different resources, predominantly from the cancer literature. Surface markers differ between humans and other species, so only human studies could be

considered (88, 89). Based on previous work, we began by isolating CD66b⁺ PBMCs as a means to obtain PMN-MDSCs for functional analysis in septic patients and healthy subjects (10). Interestingly, although we found that the purity of the isolation of CD66b⁺ leukocytes (Figure S1) was very good, and even though CD66b is considered a marker for granulocytes (90), we identified that the CD66b⁺ population consisted of a mixture of PMN- and M-MDSCs (Figure S2). Although there can be populations of MDSCs that have different levels of both CD14 or CD15 cell surface expression (91), these positively isolated CD66b⁺ PBMCs were a combination of CD14⁺CD15[−]CD66b^{low} (M-MDSC) and CD15⁺CD66b^{high} (PMN-MDSC) cells. Our CITE-seq data confirmed that *CEACAM8* expression was present in multiple myeloid cell populations. This variable MDSC cell surface expression of CD66b in septic patients appears similar to a cell type described in 1998 to define asynchronous myelopoiesis in malignant myeloid disorders (92). This highlights some of the difficulty regarding the use of cell surface phenotypes to classify MDSC subtypes after sepsis.

Of note, MDSCs are continuing to be described in certain patient populations, including sepsis, through cell surface markers only (93, 94). Although these data may be valid, our analysis would indicate that the traditional "monolithic" definition of MDSCs may not adequately define these plastic, transitory cell populations in critically ill patients with sepsis. Our results do not refute any currently accepted definitions of human MDSCs (including by cell marker phenotype) (10), but rather illustrate the complexity of the myelodysplasia that occurs after human sepsis, and the shortcomings of cell surface markers alone to identify

myeloid cell types after severe infection. In addition, other immunosuppressive cells exist in the PBMCs of whole blood from septic human patients, specifically low-density PMNs and exhausted monocytes (95, 96). This work, and our current results, indicate an immediate compelling need for more refined and nuanced descriptions and definitions of the myeloid compartment after sepsis.

Veglia et al. previously described transcriptomic differences between MDSCs and terminally differentiated monocytes and neutrophils (10). Additional guidelines for characterization and nomenclature of MDSCs based on cell surface phenotypes have been proposed, although the same central resource does not appear to exist for single-cell transcriptomic signatures of different MDSC subpopulations (11, 97). However, specific genes have been described in the literature. In cancer, *STAT3* is important for the T-cell suppression exerted by MDSCs (98). *STAT1*, -5, and -6 are also important in the regulation of arginase activity, although this may be more pertinent for cancer than sepsis based on the subdued level of *ARG1* expression in MDSCs identified from our septic patients (Figure 10) (98). It should also be noted that different subpopulations than the canonical PMN- and M-MDSCs have been previously described, including Eo-MDSCs (with eosinophilic characteristics) and fibrocystic MDSCs (99, 100).

A population of H-MDSCs was found when using the “emergent” classification system of MDSCs via genetic expression in order to classify cell types (Figure 5C). All four MDSC subpopulations appeared strongly interrelated and our data indicated that these cells are likely plastic in their myeloid state after sepsis (Figure 6B) (13). As to why we classified these cells as unique from previously defined MDSC subpopulations, H-MDSCs express many similar genes as PMN-MDSCs, although the average expression of these genes tends to be lower, such as with *IL1R2*, *CST7* and *MMP8/9*. H-MDSCs also share substantial overlap with M-MDSCs, with higher expression in sepsis of genes like *S100A8/9* and *DNAH17* (Figure 10). H-MDSCs may be an intermediary between MDSC subpopulations, and their presence in CCI further reveals the plasticity of myeloid differentiation in sepsis (Figure 8). Although MDSC subpopulations share a similar phenotype after sepsis, their function and transcriptomic patterns are distinct. Thus, after sepsis, ‘a MDSC is not a MDSC,’ and there is a unique expression of myelodysplasia after severe infection depending on both host and outcome. These data support the concept that targeted therapeutic strategies will be required within these sepsis phenotypes given the heterogenic response of the myeloid compartment to sepsis.

This study was limited by the number of patients in each study arm; however, our sample size estimates were similar to past publications in the field (14, 64). This is also a single-institution study in which treatment of sepsis is standardized but may differ compared to other institutions. Additionally, we did not stratify septic patients by septic source. Future directions include stratification of our patient cohorts by infection source and demographic information such as age, sex, and ethnicity/race to determine confounding factors which may have affected our analysis by different clinical outcomes after sepsis.

In summary, we have determined that the post-septic myeloid compartment is complex and includes a unique MDSC subpopulation that has not been previously described. Importantly, the heterogeneous response of the blood myeloid compartment to sepsis varies based on time and clinical outcome (CCI vs rapid recovery) and demonstrates that cell surface markers may not be a reliable indicator of circulating myeloid cell types after sepsis. Sepsis, like many other pathologies, requires a precision/personalized medical approach in order to improve host outcomes (22). Our work reveals specific cell types and pathways that could be modified in patients at risk of poor outcomes after sepsis (CCI) to convert them to a phenotype of rapid recovery.

Data availability statement

The datasets presented in this study can be found in online repositories. The names of the repository/repositories and accession number(s) can be found below: GSE252331 (GEO).

Ethics statement

The studies involving humans were approved by the University of Florida Institutional Review Board. The studies were conducted in accordance with the local legislation and institutional requirements. The participants provided their written informed consent to participate in this study.

Author contributions

ELB: Writing – review & editing, Writing – original draft. JRL: Writing – review & editing, Writing – original draft. DBD: Writing – review & editing, Investigation. JCR: Writing – review & editing, Investigation. MW: Writing – review & editing, Investigation. VEP: Writing – review & editing, Writing – original draft. GSG: Writing – review & editing. JAM: Writing – review & editing. MLD: Writing – review & editing, Investigation. RU: Writing – review & editing, Investigation. DCN: Writing – review & editing, Investigation. M-PLG: Writing – review & editing, Investigation. SDL: Writing – review & editing, Investigation. LM: Writing – review & editing, Investigation. TJL: Writing – review & editing, Investigation. AMM: Writing – review & editing, Investigation. RM: Writing – review & editing, Investigation. MPK: Writing – review & editing, Investigation, Funding acquisition, Conceptualization. CEM: Writing – review & editing, Investigation, Funding acquisition, Conceptualization. MAB: Writing – review & editing, Investigation. TMB: Writing – review & editing, Investigation. LLM: Writing – review & editing, Writing – original draft, Visualization, Methodology, Investigation, Conceptualization. RB: Writing – review & editing, Writing – original draft, Investigation. PAE: Supervision, Project administration, Methodology, Funding acquisition, Conceptualization, Writing – review & editing, Writing – original draft, Visualization.

Funding

The author(s) declare financial support was received for the research, authorship, and/or publication of this article. This work was supported, in part, by the following National Institutes of Health grants: National Institutes of Health grant RM1 GM139690 (LLM), National Institutes of Health grant R35 GM140806 (PE), National Institute of General Medical Sciences grant R35 GM146895 (RB), National Institute of General Medical Sciences postgraduate training grant T32 GM-008721 (EB, DD, VP, JM), National Institute of General Medical Sciences postgraduate training grant T32 HL160491 (GG).

Acknowledgments

The authors would like to thank LaShaun Bryant, BS, Brandi Buscemi, AS - Physical Therapist Assistant, Ruth Davis, BSN, Jennifer Lanz, MSN, RN, Ashley McCray, ASN, and Ivanna Rocha, MPH for their critical role with patient recruitment, retention and data collection as well as collection of human samples.

References

- Singer M, Deutschman CS, Seymour CW, Shankar-Hari M, Annane D, Bauer M, et al. The third international consensus definitions for sepsis and septic shock (Sepsis-3). *JAMA*. (2016) 315:801–10. doi: 10.1001/jama.2016.0287
- Stortz JA, Mira JC, Raymond SL, Loftus TJ, Ozrazgat-Baslanti T, Wang Z, et al. Benchmarking clinical outcomes and the immunocatabolic phenotype of chronic critical illness after sepsis in surgical intensive care unit patients. *J Trauma Acute Care Surg*. (2018) 84:342–9. doi: 10.1097/TA.0000000000001758
- Cuenca AG, Delano MJ, Kelly-Scumpia KM, Moreno C, Scumpia PO, Laface DM, et al. A paradoxical role for myeloid-derived suppressor cells in sepsis and trauma. *Mol Med*. (2011) 17:281–92. doi: 10.2119/molmed.2010.00178
- Mathias B, Delmas AL, Ozrazgat-Baslanti T, Vanzant EL, Szpila BE, Mohr AM, et al. Human myeloid-derived suppressor cells are associated with chronic immune suppression after severe sepsis/septic shock. *Ann Surg*. (2017) 265:827–34. doi: 10.1097/SLA.0000000000001783
- Horiguchi H, Loftus TJ, Hawkins RB, Raymond SL, Stortz JA, Hollen MK, et al. Innate immunity in the persistent inflammation, immunosuppression, and catabolism syndrome and its implications for therapy. *Front Immunol*. (2018) 9:595. doi: 10.3389/fimmu.2018.00595
- Kondo A, Yamashita T, Tamura H, Zhao W, Tsuji T, Shimizu M, et al. Interferon-gamma and tumor necrosis factor-alpha induce an immunoinhibitory molecule, B7-H1, via nuclear factor-kappaB activation in blasts in myelodysplastic syndromes. *Blood*. (2010) 116:1124–31. doi: 10.1182/blood-2009-12-255125
- Kondo Y, Tachikawa E, Ohtake S, Kudo K, Mizuma K, Kashimoto T, et al. Inflammatory cytokines decrease the expression of nicotinic acetylcholine receptor during the cell maturation. *Mol Cell Biochem*. (2010) 333:57–64. doi: 10.1007/s11010-009-0204-4
- Uhel F, Azzaoui I, Gregoire M, Pangault C, Dulong J, Tadie JM, et al. Early expansion of circulating granulocytic myeloid-derived suppressor cells predicts development of nosocomial infections in patients with sepsis. *Am J Respir Crit Care Med*. (2017) 196:315–27. doi: 10.1164/rccm.201606-1143OC
- Coudereau R, Waackel L, Cour M, Rimmele T, Pescarmona R, Fabri A, et al. Emergence of immunosuppressive LOX-1+ PMN-MDSC in septic shock and severe COVID-19 patients with acute respiratory distress syndrome. *J Leukocyte Biol*. (2022) 111:489–96. doi: 10.1002/JLB.4COVBCR0321-129R
- Veglia F, Sanseviero E, Gabrilovich DI. Myeloid-derived suppressor cells in the era of increasing myeloid cell diversity. *Nat Rev Immunol*. (2021) 21:485–98. doi: 10.1038/s41577-020-00490-y

Conflict of interest

The authors declare that the research was conducted in the absence of any commercial or financial relationships that could be construed as a potential conflict of interest.

The author(s) declared that they were an editorial board member of *Frontiers*, at the time of submission. This had no impact on the peer review process and the final decision.

Publisher's note

All claims expressed in this article are solely those of the authors and do not necessarily represent those of their affiliated organizations, or those of the publisher, the editors and the reviewers. Any product that may be evaluated in this article, or claim that may be made by its manufacturer, is not guaranteed or endorsed by the publisher.

Supplementary material

The Supplementary Material for this article can be found online at: <https://www.frontiersin.org/articles/10.3389/fimmu.2024.1355405/full#supplementary-material>

- Bronte V, Brandau S, Chen SH, Colombo MP, Frey AB, Greten TF, et al. Recommendations for myeloid-derived suppressor cell nomenclature and characterization standards. *Nat Commun*. (2016) 7:12150. doi: 10.1038/ncomms12150
- Mira JC, Cuschieri J, Ozrazgat-Baslanti T, Wang Z, Ghita GL, Loftus TJ, et al. The epidemiology of chronic critical illness after severe traumatic injury at two level-one trauma centers. *Crit Care Med*. (2017) 45:1989–96. doi: 10.1097/CCM.0000000000002697
- Hegde S, Leader AM, Merad M. MDSC: Markers, development, states, and unaddressed complexity. *Immunity*. (2021) 54:875–84. doi: 10.1016/j.immuni.2021.04.004
- Darden DB, Bacher R, Brusko MA, Knight P, Hawkins RB, Cox MC, et al. Single-cell RNA-seq of human myeloid-derived suppressor cells in late sepsis reveals multiple subsets with unique transcriptional responses: A pilot study. *Shock (Augusta Ga)*. (2021) 55:587–95. doi: 10.1097/SHK.0000000000001671
- Loftus TJ, Mira JC, Ozrazgat-Baslanti T, Ghita GL, Wang Z, Stortz JA, et al. Sepsis and Critical Illness Research Center investigators: protocols and standard operating procedures for a prospective cohort study of sepsis in critically ill surgical patients. *BMJ Open*. (2017) 7:e015136. doi: 10.1136/bmjopen-2016-015136
- Hollen MK, Stortz JA, Darden D, Dirain ML, Nacionales DC, Hawkins RB, et al. Myeloid-derived suppressor cell function and epigenetic expression evolves over time after surgical sepsis. *Crit Care*. (2019) 23:355. doi: 10.1186/s13054-019-2628-x
- Brakenridge SC, Efron PA, Cox MC, Stortz JA, Hawkins RB, Ghita G, et al. Current epidemiology of surgical sepsis: discordance between inpatient mortality and 1-year outcomes. *Ann Surg*. (2019) 270:502–10. doi: 10.1097/SLA.0000000000003458
- Darden DB, Brakenridge SC, Efron PA, Ghita GL, Fenner BP, Kelly LS, et al. Biomarker evidence of the persistent inflammation, immunosuppression and catabolism syndrome (PICS) in chronic critical illness (CCI) after surgical sepsis. *Ann Surg*. (2021) 274:664–73. doi: 10.1097/SLA.0000000000005067
- Trellakis S, Bruderek K, Hutte J, Elian M, Hoffmann TK, Lang S, et al. Granulocytic myeloid-derived suppressor cells are cryosensitive and their frequency does not correlate with serum concentrations of colony-stimulating factors in head and neck cancer. *Innate Immun*. (2013) 19:328–36. doi: 10.1177/1753425912463618
- Blanter M, Gouwy M, Struyf S. Studying neutrophil function *in vitro*: cell models and environmental factors. *J Inflammation Res*. (2021) 14:141–62. doi: 10.2147/JIR.S284941
- Schenz J, Obermaier M, Uhle S, Weigand MA, Uhle F. Low-density granulocyte contamination from peripheral blood mononuclear cells of patients with sepsis and

- how to remove it - A technical report. *Front Immunol.* (2021) 12:684119. doi: 10.3389/fimmu.2021.684119
22. Darden DB, Kelly LS, Fenner BP, Moldawer LL, Mohr AM, Efron PA. Dysregulated immunity and immunotherapy after sepsis. *J Clin Med.* (2021) 10. doi: 10.3390/jcm10081742
23. Zheng GX, Terry JM, Belgrader P, Ryvkin P, Bent ZW, Wilson R, et al. Massively parallel digital transcriptional profiling of single cells. *Nat Commun.* (2017) 8:14049. doi: 10.1038/ncomms14049
24. Andrews S. A quality control tool for high throughput sequence data: Babraham Bioinformatics (2010). Available online at: <https://www.bioinformatics.babraham.ac.uk/projects/fastqc/>.
25. Gaidatzis D, Burger L, Florescu M, Stadler MB. Analysis of intronic and exonic reads in RNA-seq data characterizes transcriptional and post-transcriptional regulation. *Nat Biotechnol.* (2015) 33:722–9. doi: 10.1038/nbt.3269
26. Srivastava A, Malik L, Sarkar H, Patro R. A Bayesian framework for inter-cellular information sharing improves dscRNA-seq quantification. *Bioinformatics.* (2020) 36: i292–i9. doi: 10.1093/bioinformatics/btaa450
27. Srivastava A, Malik L, Smith T, Sudbery I, Patro R. Alevin efficiently estimates accurate gene abundances from dscRNA-seq data. *Genome Biol.* (2019) 20:65. doi: 10.1186/s13059-019-1670-y
28. He D, Zakeri M, Sarkar H, Soneson C, Srivastava A, Patro R. Alevin-fry unlocks rapid, accurate and memory-frugal quantification of single-cell RNA-seq data. *Nat Methods.* (2022) 19:316–22. doi: 10.1038/s41592-022-01408-3
29. R. A language and environment for statistical computing.: The R Foundation (2022). Available online at: <https://www.r-project.org/>.
30. Python language reference: python (2019). Available online at: <https://docs.python.org/3/>.
31. Zhu A, Srivastava A, Ibrahim JG, Patro R, Love MI. Nonparametric expression analysis using inferential replicate counts. *Nucleic Acids Res.* (2019) 47:e105. doi: 10.1093/nar/gkz622
32. Griffiths JA, Richard AC, Bach K, Lun ATL, Marioni JC. Detection and removal of barcode swapping in single-cell RNA-seq data. *Nat Commun.* (2018) 9:2667. doi: 10.1038/s41467-018-05083-x
33. Lun ATL, Riesenfeld S, Andrews T, Dao TP, Gomes Tparticipants in the 1st Human Cell Atlas J, et al. EmptyDrops: distinguishing cells from empty droplets in droplet-based single-cell RNA sequencing data. *Genome Biol.* (2019) 20:63. doi: 10.1186/s13059-019-1662-y
34. Hao Y, Hao S, Andersen-Nissen E, Mauck WM 3rd, Zheng S, Butler A, et al. Integrated analysis of multimodal single-cell data. *Cell.* (2021) 184:3573–87 e29. doi: 10.1016/j.cell.2021.04.048
35. Tirosh I, Izar B, Prakadan SM, Wadsworth MH 2nd, Treacy D, Trombetta JJ, et al. Dissecting the multicellular ecosystem of metastatic melanoma by single-cell RNA-seq. *Science.* (2016) 352:189–96. doi: 10.1126/science.aad0501
36. Korsunsky I, Millard N, Fan J, Slowikowski K, Zhang F, Wei K, et al. Fast, sensitive and accurate integration of single-cell data with Harmony. *Nat Methods.* (2019) 16:1289–96. doi: 10.1038/s41592-019-0619-0
37. McInnes LHJ, Melville J. UMAP: uniform manifold Approximation and Projection for Dimension Reduction. Cornell University (2018). Available online at: <https://arxiv.org/abs/1802.03426>.
38. Blondel VD, Guillaume J-L, Lambiotte R, Lefebvre E. Fast unfolding of communities in large networks. *J Stat Mechanics: Theory Experiment.* (2008) 2008: P10008. doi: 10.1088/1742-5468/2008/10/P10008
39. Aran D, Looney AP, Liu L, Wu E, Fong V, Hsu A, et al. Reference-based analysis of lung single-cell sequencing reveals a transitional profibrotic macrophage. *Nat Immunol.* (2019) 20:163–72. doi: 10.1038/s41590-018-0276-y
40. Schmiedel BJ, Singh D, Madrigal A, Valdovino-Gonzalez AG, White BM, Zapardiel-Gonzalo J, et al. Impact of genetic polymorphisms on human immune cell gene expression. *Cell.* (2018) 175:1701–15 e16. doi: 10.1016/j.cell.2018.10.022
41. Martens JH, Stunnenberg HG. BLUEPRINT: mapping human blood cell epigenomes. *Haematologica.* (2013) 98:1487–9. doi: 10.3324/haematol.2013.094243
42. Consortium EP. An integrated encyclopedia of DNA elements in the human genome. *Nature.* (2012) 489:57–74. doi: 10.1038/nature11247
43. Mabbott NA, Baillie JK, Brown H, Freeman TC, Hume DA. An expression atlas of human primary cells: inference of gene function from coexpression networks. *BMC Genomics.* (2013) 14:632. doi: 10.1186/1471-2164-14-632
44. Monaco G, Lee B, Xu W, Mustafah S, Hwang YY, Carre C, et al. RNA-seq signatures normalized by mRNA abundance allow absolute deconvolution of human immune cell types. *Cell Rep.* (2019) 26:1627–40 e7. doi: 10.1016/j.celrep.2019.01.041
45. Bauer DF. Constructing confidence sets using rank statistics. *J Am Stat Assoc.* (1972) 67:687–90. doi: 10.1080/01621459.1972.10481279
46. Miller RG. *Simultaneous statistical inference.* 2nd ed. New York, NY: Springer International Publishing (2012). p. 315.
47. Crowell HL, Soneson C, Germain PL, Calini D, Collin L, Raposo C, et al. muscat detects subpopulation-specific state transitions from multi-sample multi-condition single-cell transcriptomics data. *Nat Commun.* (2020) 11:6077. doi: 10.1038/s41467-020-19894-4
48. Benzanson JE, Karpinski S, Shah VB. Julia: A fresh approach to numerical computing. *SIAM Rev.* (2017) 59:65–98. doi: 10.1137/141000671
49. Bates DA, Kleinschmidt D, Calderon JBS, Noack A, Kelman T, Bouchet-Valat M, et al. *JuliaStats/MixedModels.jl: v2.3.0 (v.2.3.0)*. Zenodo (2020). doi: 10.5281/zenodo.3727845
50. Holm S. A simple sequentially rejective multiple test procedure. *Scand J Stat.* (1979) 6:65–70. Available at: <http://www.jstor.org/stable/4615733>
51. Kolberg L, Raudvere U, Kuzmin I, Vilo J, Peterson H. gprofiler2 – an R package for gene list functional enrichment analysis and namespace conversion toolset g: Profiler. *F1000Res.* (2020) 9. doi: 10.12688/f1000research
52. Bhuva DD. vissE: Visualising Set Enrichment Analysis Results (2022). Available online at: <https://davislaboratory.github.io/vissE>.
53. Melville J. uwot: The Uniform Manifold Approximation and Projection (UMAP) method for dimensionality reduction (2022). Available online at: <https://CRAN.R-project.org/package=uwot>.
54. Virshup I, Rybakov S, Theis FJ, Angerer P, Wolf FA. anndata: annotated data. *bioRxiv.* (2021), 2021.12.16.473007. doi: 10.1101/2021.12.16.473007
55. La Manno G, Soldatov R, Zeisel A, Braun E, Hochgerner H, Petukhov V, et al. RNA velocity of single cells. *Nature.* (2018) 560:494–8. doi: 10.1038/s41586-018-0414-6
56. Bergen V, Lange M, Peidli S, Wolf FA, Theis FJ. Generalizing RNA velocity to transient cell states through dynamical modeling. *Nat Biotechnol.* (2020) 38:1408–14. doi: 10.1038/s41587-020-0591-3
57. Lange M, Bergen V, Klein M, Setty M, Reuter B, Bakhti M, et al. CellRank for directed single-cell fate mapping. *Nat Methods.* (2022) 19:159–70. doi: 10.1038/s41592-021-01346-6
58. Wolf FA, Hamey FK, Plass M, Solana J, Dahlin JS, Gottgens B, et al. PAGA: graph abstraction reconciles clustering with trajectory inference through a topology preserving map of single cells. *Genome Biol.* (2019) 20:59. doi: 10.1186/s13059-019-1663-x
59. Wolf FA, Angerer P, Theis FJ. SCANPY: large-scale single-cell gene expression data analysis. *Genome Biol.* (2018) 19:15. doi: 10.1186/s13059-017-1382-0
60. Jacomy M, Venturini T, Heymann S, Bastian M. ForceAtlas2, a continuous graph layout algorithm for handy network visualization designed for the Gephi software. *PLoS One.* (2014) 9:e98679. doi: 10.1371/journal.pone.0098679
61. Fruchterman TMJ, Reingold EM. Graph drawing by force-directed placement. *Software: Pract Experience.* (1991) 21:1129–64. doi: 10.1002/spe.4380211102
62. Pinheiro JCBDMRCT. nlme: linear and nonlinear mixed Effects Models (2023). Available online at: <https://CRAN.R-project.org/package=nlme>.
63. Lenth RVBBB, P., Gine-Vazquez I, Herve M, Jung M, Love J, Miguez F, et al. emmeans: Estimated Marginal Means, aka Least-Squares Means (2023). Available online at: <https://CRAN.R-project.org/package=emmeans>.
64. Darden DB, Dong X, Brusko MA, Kelly L, Fenner B, Rincon JC, et al. A Novel single cell RNA-seq analysis of non-myeloid circulating cells in late sepsis. *Front Immunol.* (2021) 12:696536. doi: 10.3389/fimmu.2021.696536
65. Stoeckius M, Hafemeister C, Stephenson W, Houck-Loomis B, Chattopadhyay PK, Swerdlow H, et al. Simultaneous epitope and transcriptome measurement in single cells. *Nat Methods.* (2017) 14:865–8. doi: 10.1038/nmeth.4380
66. Gabrilovich DI. Myeloid-derived suppressor cells. *Cancer Immunol Res.* (2017) 5:3–8. doi: 10.1158/2326-6066.CIR-16-0297
67. Luperto M, Zafrani L. T cell dysregulation in inflammatory diseases in ICU. *Intensive Care Med Exp.* (2022) 10:43. doi: 10.1186/s40635-022-00471-6
68. Rincon JC, Efron PA, Moldawer LL. Immunopathology of chronic critical illness in sepsis survivors: Role of abnormal myelopoiesis. *J Leukoc Biol.* (2022) 112:1525–34. doi: 10.1002/JLB.4MR0922-690RR
69. Pray BA, Youssef Y, Alinari L. TBL1X: At the crossroads of transcriptional and posttranscriptional regulation. *Exp Hematol.* (2022) 116:18–25. doi: 10.1016/j.exphem.2022.09.006
70. Itskovich SS, Gurunathan A, Clark J, Burwinkel M, Wunderlich M, Berger MR, et al. MBNL1 regulates essential alternative RNA splicing patterns in MLL-rearranged leukemia. *Nat Commun.* (2020) 11:2369. doi: 10.1038/s41467-020-15733-8
71. Zhang Q, Wu Y, Chen J, Tan F, Mou J, Du Z, et al. The regulatory role of both MBNL1 and MBNL1-AS1 in several common cancers. *Curr Pharm Des.* (2022) 28:581–5. doi: 10.2174/1381612827666210830110732
72. Li X, Li Y, Yu Q, Qian P, Huang H, Lin Y. Metabolic reprogramming of myeloid-derived suppressor cells: An innovative approach confronting challenges. *J Leukoc Biol.* (2021) 110:257–70. doi: 10.1002/JLB.1MR0421-597RR
73. Santos SS, Carmo AM, Brunialti MK, MaChado FR, Azevedo LC, Assuncao M, et al. Modulation of monocytes in septic patients: preserved phagocytic activity, increased ROS and NO generation, and decreased production of inflammatory cytokines. *Intensive Care Med Exp.* (2016) 4:5. doi: 10.1186/s40635-016-0078-1
74. Gong FC, Ji R, Wang YM, Yang ZT, Chen Y, Mao EQ, et al. Identification of potential biomarkers and immune features of sepsis using bioinformatics analysis. *Mediators Inflamm.* (2020) 2020:3432587. doi: 10.1155/2020/3432587
75. Wu W, Zhang X, Lv H, Liao Y, Zhang W, Cheng H, et al. Identification of immediate early response protein 2 as a regulator of angiogenesis through the modulation of endothelial cell motility and adhesion. *Int J Mol Med.* (2015) 36:1104–10. doi: 10.3892/ijmm.2015.2310

76. Kyjacova L, Saup R, Ronsch K, Wallbaum S, Dukowic-Schulze S, Foss A, et al. IER2-induced senescence drives melanoma invasion through osteopontin. *Oncogene*. (2021) 40:6494–512. doi: 10.1038/s41388-021-02027-6
77. Chung TP, Laramie JM, Meyer DJ, Downey T, Tam LH, Ding H, et al. Molecular diagnostics in sepsis: from bedside to bench. *J Am Coll Surg*. (2006) 203:585–98. doi: 10.1016/j.jamcollsurg.2006.06.028
78. Gabrilovich DI, Bronte V, Chen SH, Colombo MP, Ochoa A, Ostrand-Rosenberg S, et al. The terminology issue for myeloid-derived suppressor cells. *Cancer Res*. (2007) 67:425; author reply 6. doi: 10.1158/0008-5472.CAN-06-3037
79. Veglia F, Perego M, Gabrilovich D. Myeloid-derived suppressor cells coming of age. *Nat Immunol*. (2018) 19:108–19. doi: 10.1038/s41590-017-0022-x
80. Li K, Shi H, Zhang B, Ou X, Ma Q, Chen Y, et al. Myeloid-derived suppressor cells as immunosuppressive regulators and therapeutic targets in cancer. *Signal Transduct Target Ther*. (2021) 6:362. doi: 10.1038/s41392-021-00670-9
81. Kotze LA, van der Spuy G, Leonard B, Penn-Nicholson A, Musvosvi M, McAnda S, et al. Targeted gene expression profiling of human myeloid cells from blood and lung compartments of patients with tuberculosis and other lung diseases. *Front Immunol*. (2022) 13:839747. doi: 10.3389/fimmu.2022.839747
82. Dean MJ, Ochoa JB, Sanchez-Pino MD, Zabaleta J, Garai J, Del Valle L, et al. Severe COVID-19 is characterized by an impaired type I interferon response and elevated levels of arginase producing granulocytic myeloid derived suppressor cells. *Front Immunol*. (2021) 12:695972. doi: 10.3389/fimmu.2021.695972
83. Chen L, Jin S, Yang M, Gui C, Yuan Y, Dong G, et al. Integrated single cell and bulk RNA-seq analysis revealed immunomodulatory effects of ulinastatin in sepsis: A multicenter cohort study. *Front Immunol*. (2022) 13:882774. doi: 10.3389/fimmu.2022.882774
84. Schulte-Schrepping J, Reusch N, Paclik D, Bassler K, Schlickeiser S, Zhang B, et al. Severe COVID-19 is marked by a dysregulated myeloid cell compartment. *Cell*. (2020) 182:1419–40 e23. doi: 10.1016/j.cell.2020.08.001
85. Kiaee F, Jamaati H, Shahi H, Roofchayee ND, Varahram M, Folkerts G, et al. Immunophenotype and function of circulating myeloid derived suppressor cells in COVID-19 patients. *Sci Rep*. (2022) 12:22570. doi: 10.1038/s41598-022-26943-z
86. Xu G, Qi F, Li H, Yang Q, Wang H, Wang X, et al. The differential immune responses to COVID-19 in peripheral and lung revealed by single-cell RNA sequencing. *Cell Discovery*. (2020) 6:73. doi: 10.1038/s41421-020-00225-2
87. Rowlands M, Segal F, Hartl D. Myeloid-derived suppressor cells as a potential biomarker and therapeutic target in COVID-19. *Front Immunol*. (2021) 12:697405. doi: 10.3389/fimmu.2021.697405
88. Fridlender ZG, Sun J, Mishalian I, Singhal S, Cheng G, Kapoor V, et al. Transcriptomic analysis comparing tumor-associated neutrophils with granulocytic myeloid-derived suppressor cells and normal neutrophils. *PLoS One*. (2012) 7:e31524. doi: 10.1371/journal.pone.0031524
89. Millrud CR, Bergenfelz C, Leandersson K. On the origin of myeloid-derived suppressor cells. *Oncotarget*. (2017) 8:3649–65. doi: 10.18632/oncotarget.v8i2
90. McKenna E, Mhaonaigh AU, Wubben R, Dwivedi A, Hurley T, Kelly LA, et al. Neutrophils: need for standardized nomenclature. *Front Immunol*. (2021) 12:602963. doi: 10.3389/fimmu.2021.602963
91. Vetsika EK, Koinis F, Gioulbasani M, Aggouraki D, Koutoulaki A, Skolidaki E, et al. A circulating subpopulation of monocytic myeloid-derived suppressor cells as an independent prognostic/predictive factor in untreated non-small lung cancer patients. *J Immunol Res*. (2014) 2014:659294. doi: 10.1155/2014/659294
92. Hansen I, Meyer K, Hokland P. Flow cytometric identification of myeloid disorders by asynchronous expression of the CD14 and CD66 antigens. *Eur J Haematol*. (1998) 61:339–46. doi: 10.1111/j.1600-0609.1998.tb01098.x
93. Feng S, Cui Y, Zhou Y, Shao L, Miao H, Dou J, et al. Continuous renal replacement therapy attenuates polymorphonuclear myeloid-derived suppressor cell expansion in pediatric severe sepsis. *Front Immunol*. (2022) 13:990522. doi: 10.3389/fimmu.2022.990522
94. De Zuani M, Hortova-Kohoutkova M, Andrejcinova I, Tomaskova V, Sramek V, Helan M, et al. Human myeloid-derived suppressor cell expansion during sepsis is revealed by unsupervised clustering of flow cytometric data. *Eur J Immunol*. (2021) 51:1785–91. doi: 10.1002/eji.202049141
95. Sun R, Huang J, Yang Y, Liu L, Shao Y, Li L, et al. Dysfunction of low-density neutrophils in peripheral circulation in patients with sepsis. *Sci Rep*. (2022) 12:685. doi: 10.1038/s41598-021-04682-x
96. Pradhan K, Yi Z, Geng S, Li L. Development of exhausted memory monocytes and underlying mechanisms. *Front Immunol*. (2021) 12:778830. doi: 10.3389/fimmu.2021.778830
97. Bergenfelz C, Leandersson K. The generation and identity of human myeloid-derived suppressor cells. *Front Oncol*. (2020) 10:109. doi: 10.3389/fonc.2020.00109
98. Condamine T, Gabrilovich DI. Molecular mechanisms regulating myeloid-derived suppressor cell differentiation and function. *Trends Immunol*. (2011) 32:19–25. doi: 10.1016/j.it.2010.10.002
99. Goldmann O, Beineke A, Medina E. Identification of a novel subset of myeloid-derived suppressor cells during chronic staphylococcal infection that resembles immature eosinophils. *J Infect Dis*. (2017) 216:1444–51. doi: 10.1093/infdis/jix494
100. Zhang H, Maric I, DiPrima MJ, Khan J, Orentas RJ, Kaplan RN, et al. Fibrocytes represent a novel MDSC subset circulating in patients with metastatic cancer. *Blood*. (2013) 122:1105–13. doi: 10.1182/blood-2012-08-449413